Submitted to Metallurgical and Materials Transactions A [October 2015]: J.C.M. Li Symposium

The Strength-Grain Size Relationship in Ultrafine-Grained Metals

N. Balasubramanian[1] and Terence G. Langdon[2,3]

N. BALASUBRAMANIAN is Visiting Scholar and TERENCE G. LANGDON is Emeritus Professor in the Departments of Aerospace & Mechanical Engineering and Materials Science, University of Southern California, Los Angeles, CA 90089-1453.

Corresponding author: Terence G. Langdon, e-mail: langdon@usc.edu

Abstract

Metals processed by severe plastic deformation [SPD] techniques, such as equal-channel angular pressing [ECAP] and high-pressure torsion [HPT], generally have submicrometer grain sizes. Consequently, they exhibit high strength as expected on the basis of the Hall-Petch [H-P] relationship. Examples of this behavior are discussed using data on Ti, Al-Mg

and Ni. These materials typically have grain size above ~50 nm where softening is not expected. An increase in strength is usually accompanied by a decrease in ductility. High strength and ductility can be achieved simultaneously by imposing high strains to give both ultrafine grain sizes and a high fraction of high-angle grain boundaries. An example is presented for a cast Al-7% Si alloy processed by HPT. In some cases, SPD may produce a fine grain size but also lead to a weakening due to microstructural changes as in ECAP of an Al-7034 alloy and HPT of Zn-22% Al. In SPD-processed materials, grain boundary segregation and nanostructural features are present which may lead to higher strengths than those predicted by the H-P relationship in some alloys having nano grain sizes.

Keywords: grain boundary sliding; Hall-Petch relationship; severe plastic deformation,; strength and ductility; ultrafine grains.

PREAMBLE

It is a very great pleasure for us to have this opportunity to prepare this report in tribute to Professor James C.M. Li on his 90th birthday. One of the authors [NB] was one of the earliest graduate students working on his doctoral thesis under the direction of Professor Li at Columbia University. He obtained his D.Eng.Sci. degree in 1970. The other author [TGL] worked with Li at the Edgar C. Bain Laboratory of the U.S. Steel Corporation in Monroeville, PA, in 1967/68. Both of us have retained very close friendship with Li over the last forty years. Strength, deformation and the role of grain size and grain boundaries are the research areas where Li has made significant contributions. Accordingly, we have chosen this topic for our paper as this special tribute.

I. INTRODUCTION

It is well established that the grain size plays a predominant role in developing the mechanical properties of materials. [1,2] The strength of a polycrystalline material depends on grain size as shown by the Hall-Petch [H-P] relationship[3,4] which relates the yield stress, σ_y, to the grain size, d:

$$\sigma_y = \sigma_o + k_y d^{-1/2} \qquad [1]$$

where σ_o is a lattice friction stress and k_y is a constant of yielding. In addition, small grain sizes give rise to superplastic flow at high temperatures [5-7] so that complex shapes are easily formed as in the superplastic forming industry.[8]

With smaller grain sizes, the strain rates for superplasticity are increased and this leads to higher productivity by processing objects in shorter times or to the possibility of achieving

superplasticity at lower temperatures giving energy savings. This follows from the equation for the superplastic strain rate, $\dot{\varepsilon}_{sp}$, which is given by [9]

$$\dot{\varepsilon}_{sp} = \frac{AD_{gb}G\mathbf{b}}{kT}\left(\frac{\mathbf{b}}{d}\right)^2\left(\frac{\sigma}{G}\right)^2 \qquad [2]$$

where D_{gb} is the coefficient for grain boundary diffusion, G is the shear modulus, **b** is the Burgers vector, k is Boltzmann's constant, T is the absolute temperature and σ is the flow stress. The dependence on temperature is expressed in terms of T and D_{gb} which contains an Arrhenius term. In the equation, the activation energy for superplastic flow is identified as the activation energy for grain boundary diffusion, Q_{gb}, and the relationship was proposed for conventional superplastic materials based on a model in which grain boundary sliding is the mechanism for superplasticity with accommodation by intragranular slip. In practice, however, this same relationship applies also to ultrafine-grain [UFG] metals and this is illustrated in Figs 1[a] and [b] where experimental data are plotted for a wide range of Al and Mg alloys using data obtained by equal-channel angular pressing [ECAP] and high-pressure torsion [HPT]. [7, 10] The experimental results shown in Fig. 1[a] are taken from various reports for Al alloys,[11-29] and in Fig. 1[b] there are similar sets of data for a range of Mg alloys[30-49] where the upper solid lines in Figs 1[a] and [b] show the predicted normalized strain rates derived using eq. [2]. It is readily apparent that all datum points for both sets of alloys lie close to the theoretical lines and similar results are obtained when processing by either ECAP or HPT. Thus, there is generally very good agreement with the theoretical model.

In view of the importance of grain size, there have been several efforts historically to obtain small grain sizes by thermo-mechanical processing [TMP] and generally this permits the refinement of grain sizes to the order of a few micrometers. Nevertheless, TMP is not capable of producing grain sizes below 1 μm and therefore alternative approaches are necessary. Several procedures are now available which can produce submicrometer of even nanometer grain sizes where these procedures are based on the application of severe plastic deformation [SPD] which imposes a high strain on the specimens without any changes in the overall dimensions of the samples.[50,51] Thus, ECAP involves pressing a rod or bar through a die which is constrained within a channel bent through a specified angle[52,53] and HPT involves the processing of thin disks which are subjected to high applied pressures and then concurrent torsional straining.[54] In general, ECAP produces grain sizes in the submicrometer range whereas, since a very high shear strain is imposed on the sample in HPT, it is possible to use this technique to produce grain sizes in the nanometer range. There are also several other methods of SPD processing such as equal-channel forward extrusion, [55] accumulative roll bonding, [56] surface mechanical attrition treatment [57] and repeated corrugation and straightening[58]. Methods are also available for producing metals with grain sizes in the nanometer range that do not involve SPD processing such as in the use of electroplating. [59] Recently, a 5 nm grain size was obtained in Cu by applying a large sliding load in liquid nitrogen.[60]

Many experimental results are now available on UFG materials and the techniques for characterizing them have also been developed. Nevertheless, there are some problems that need to be addressed such as the limited ductility that is generally achieved in these high strength metals. There are also questions regarding possible deviations from the Hall-

Petch relationship at the nanometer level, the detailed nature of the flow mechanisms involving grain boundary sliding and dislocation emission and accumulation and the nature and role of the grain boundaries formed in SPD processing such as non-equilibrium boundaries and high-angle grain boundaries [HAGB} defined as those having misorientation angles of ≥15°. These questions are examined in the following sections based on recent data and concepts.

II. THE HALL-PETCH RELATIONSHIP FOR UFG MATERIALS

The yield point[61-63] and associated phenomena like Lüders bands[64,65] were for a long time considered specific to iron and steel. But with the development of materials with smaller grain sizes it was possible to observe these phenomena in fcc materials also. It was shown in alpha brass with 13, 20 and 30% Zn and a grain size of 20 μm that yielding occurred by propagation of a Lüders band.[66] The velocity of Lüders band propagation was measured as a function of stress and it followed a power law with an exponent equal to the dislocation velocity–stress exponent. With the advent of UFG materials, discontinuous yielding and Lüders band deformation was observed in Al,[67] Cu,[68] Mg,[69] Ti[70,71] and alloys[68,72] in addition to austenitic steels.[73] Closely linked to this topic is the yield stress and its dependence on grain size. In general, materials not processed by SPD have a lower slope for k_y in eq. [1]. Experimental data, which is also in reasonable agreement with theoretical calculations, show that the values of k_y [in units of $MPa.mm^{1/2}$] are 1.4, 4.9, 5.0 and 0.43 for Al, Ni, Cu and Fe, respectively.[74] The SPD-processed materials have higher values as discussed in the following sections, and a high entropy alloy CoCrFeNiMn with a grain size of 40 nm has a value of 27.7.[75]

A. The Hall-Petch Relation in Pure Ti

Pure Ti is preferred over Ti alloys in bio-medical applications. Accordingly, there is a significant motivation to increase the strength of commercially pure Ti by SPD processing in order to match the strength of alloys such as Ti-6Al-4V. The finer grain size after SPD processing indeed contributes to strength and Fig. 2 shows that the H-P relation is valid down to 9 nm in commercially pure Ti where the yield stress [YS] is taken as 1/3rd of the measured microhardness.[76] Based on five investigations,[76-80] the average H–P slope is ~13 MPa $mm^{½}$. A combination of HPT at 5.0 GPa for 10 rotations followed by annealing at 523-273 K (250-300°C) gives more than 1200 MPa in pure Ti with a grain size of 120 nm and this is comparable to the reported strengths of Ti alloys.

A compilation[81] of results on the H-P relation in Ti from a wide range of investigations[82-100] is shown in Fig. 3 where the designations of Grades 1 to 4 mean increasing impurity contents of Fe, N and O which thereby increase the strength. It is apparent that the YS is improved by SPD in all cases. A Grade 4 Ti after HPT at 6.0 GPa and 10 rotations gave the highest strength of 1450 MPa with a grain size of 110 nm.[99] In addition, a comparison of the tribocorrosion performances of coarse-grained and UFG Ti showed improved wear resistance in the UFG Ti with less plastic deformation under high contact pressures.[101]

A recent experimental report described the use of ECAP to consolidate chips from the machining of Ti.[102] These experiments gave σ_o = 182 MPa and k_y = 11.4 MPa.$mm^{1/2}$ in the H-P relationship. The strengthening was attributed to low-angle grain boundaries [LAGBs], high-angle grain boundaries [HAGBs], oxide dispersions and solid solution strengthening in addition

to the Peierls-Nabarro contribution. The contribution from HAGBs followed the H-P relation and the calculated values of strength agreed with the experimental values.

B. The Hall-Petch Relation in Al alloys

There have been many studies on Al alloys but imposed strains are often insufficient to achieve exceptional strengthening. For example, processing by HPT is often limited to only 5 turns. It is now understood that larger numbers of turns may change the character of the grain boundaries even after reaching a reasonable saturation smallest grain size. Thus, with increasing numbers of turns a larger fraction of LAGBs turn into HAGBs and the mechanical properties improve. This is shown by very recent results on an Al-5% Mg alloy [AA 5483][103] where the results are summarized in Fig. 4 for microhardness data in the coarse-grained material and after processing by HPT at 6.0 GPa by ¼ to 10 turns. Except for the data at ¼, ½ and 1 turn, all results, including for the coarse-grained alloy, are well represented by the equation:

$$H = H_o + k_H d^{-1/2} \qquad [3]$$

where H is the hardness and H_o and k_H are material constants.

The data in Fig. 4 show that H_o is ~72 and k_H is estimated as ~1430 Hv.nm$^{1/2}$. This corresponds to $\sigma_o \approx 240$ MPa and $k_y \approx 4.7$ MPa.mm$^{1/2}$. The coarse-grained samples of the same material were obtained by annealing the initial alloy at 573 K for one hour and at 673 K for one and five hours and then plotting as shown in Fig. 4. Thus, all HPT results for the coarse and fine grain sizes lie on the same line with the exception of the samples processed by HPT through ¼, ½ and 1 turn where the datum points fall below the line. After small numbers of turns there are significant variations both in the distributions of the individual grain sizes and in the grain boundary character distributions as demonstrated by measurements of the boundary misorientation angles. For SPD-processed materials, the grain boundaries differ in their misorientation angles as a

direct consequence of the microstructural evolution that occurs during processing. Thus, as the applied strain increases, the distributions in the misorientation angles are shifted to higher values so that the fractions of HAGBs increases from about 55% to 80% when increasing the torsional straining from ½ to 10 turns, respectively.

It is well established that slip transfer through LAGBs is much easier by comparison with HAGBs and therefore they represent weaker barriers for the movement of lattice dislocations. The present results are consistent with a phenomenological model in which the HAGBs are strengthening elements within the microstructure whereas the LAGBs make only a minor contribution to the strength of the material.[104] The stress is enhanced at HAGBs due to the formation of dislocation pile-ups and yielding that take place when the stress is sufficiently large to initiate slip from one grain to the next. In this model, the LAGBs are then less effective in impeding dislocation slip due to the relatively smaller crystallographic misalignment across the grain boundaries.

An earlier study reported $\sigma_o \approx 62$ MPa and $k_y \approx 4.7$ MPa.mm$^{1/2}$ in an Al-3% Mg alloy processed by ECAP.[105] However, in processing of this alloy by HPT there was a decrease in the H-P slope at a grain size of ~150 nm.[106] Using accumulative roll bonding, there are reports of $\sigma_o \approx 6$ MPa and $k_y \approx 3.3$ MPa.mm$^{1/2}$ for Al 1100.[107] In practice, the slopes for UFG materials are generally higher than for materials not so processed so that, for example, there is a reported value of $k_y \approx 1.1$ MPa.mm$^{1/2}$ for a coarse grain Al.[74]

III. OBSERVATIONS ON THE PARADOX OF STRENGTH AND DUCTILITY

It is generally true that materials having high strength also have poor ductility.[108] Furthermore, this problem is enhanced in UFG materials because of their low rate of strain hardening and low

strain rate sensitivity. The situation is admirably summarized in Fig. 5 which plots the YS against the measured elongation to failure for a number of metals where the numbers next to the lines for Al and Cu denote the strains imposed during rolling and the two points labeled nano Ti and nano Cu are nanostructured metals processed through 5 turns of HPT and 16 passes of ECAP, respectively.[109] Plastic instability is initiated when the stress, σ, exceeds the strain hardening coefficient, $d\sigma/d\varepsilon$, where ε is the strain. Hence, localized deformation may be shifted to higher stresses if the strain hardening coefficient is high. In practice, much research has focused on the problem of ductility since other mechanical properties of industrial importance, such as fatigue and fracture strength, also depend on ductility. Methods have been developed which are specific to some materials such as short term [~10 minutes] anneals after ECAP for Cu[110] and Ti,[111,112] or after HPT for Ta[113] and an Al-1% Mg alloy.[114] The principle of this approach is to equilibrate the grain boundaries after SPD without incurring any significant grain growth and thereby to move dislocations from the grain interiors to the grain boundaries so that strain hardening is increased leading to higher ductility.

A more general method is simply to increase the numbers of rotations in HPT so that, even after the grain size has been reduced and reasonably saturated, the fraction of HAGBs is further increased. In Fig. 5, the nano Cu after 16 passes of ECAP and nano Ti after 5 turns of HPT are two examples of this approach since these nanomaterials have both high strength and high ductility.[109] The paradox of strength and ductility may be addressed also through a combination of HPT and other strategies such as the chemical composition for lattice softening and the development of a multimodal structure consisting of equiaxed nanograins, lamellar coarse grains and fine precipitates.[115] The Fe-Ni-Al-C alloy was designed with an ultrahigh strength of ~1.9 to 2.2 GPa and a uniform ductility of ~16-19% after HPT at 6.0 GPa and 50 turns.[115] These

results, as well as other examples using the above strategies,[116-120] are shown in Fig. 6 using the same conventional display as in Fig. 5.[115]

In Figs 5 and 6 the curve separating the new and improved nanostructured materials at upper right from the conventional materials at lower left is schematic and qualitative. This means it is not well defined and this type of plot cannot be used for a rigorous evaluation of strength and ductility characteristics. To overcome this limitation, a quantitative approach was developed recently in which the data are plotted in terms of the normalized yield stress, YS [or the ultimate tensile stress, UTS], against the normalized uniform elongation [or the normalized elongation to failure].[121] This normlization is conducted with reference to the starting material which is represented by co-ordinates [1,1] as shown in Fig. 7. Using this approach, conventional materials then fall to the left of the vertical broken line or below the horizontal broken line as shown in the shaded area whereas materials exhibiting high strength and high ductility [HSHD] lie in the area at the upper right of the diagram where both co-ordinates simultaneously have values greater than 1.

This procedure may be illustrated using results from a thorough investigation of a cast Al -7% Si alloy which is a material used in automotive applications where an increase in ductility will be profitable.[121] This alloy was processed by HPT at 6.0 GPa up to 10 turns at temperatures of 298 K (25°C) or 445 K (172°C), the processed grain size was ~0.4 μm, the strain rate sensitivity increased with increasing numbers of HPT turns from ~0.03 to ~0.14 and the average Si particle size was reduced from ~2.8 to ~0.12 μm after 5 cycles of HPT.[122] Figure 8 shows representative curves of engineering stress versus engineering strain for the material processed by HPT at 298 K (25°C) for different numbers of turns and then tested at room temperature [298 K (25°C)] at a strain rate of 1.0×10^{-3} s^{-1}. It is apparent from Fig. 8 that the values of YS and

UTS increase in value even after ¼ rotation and the highest elongations to failure are achieved after 5 to 10 turns. Results from the tests at four different strain rates are shown in Fig. 9 using the new quantitative diagram with normalized coordinates. Although there are a few datum points lying in the region of conventional behavior, there are several points that lie clearly in the region at upper right denoting HSHD. By contrast, experiments showed that short-term annealing after SPD increased the elongation but not sufficiently to move the datum into the HSHD region in materials such as the Al-1% Mg alloy.[121] Thus, the quantitative diagram in Fig. 7 is a useful tool for assessing different materials and processing methods when attempting to achieve HSHD.

A fundamental question concerns the explanation for the superior ductility that may be achieved when nanomaterials are processed by many passes of ECAP or many turns of HTP. There are three significant observations that shed light on this question and identify the features promoting ductility. Firstly, even after reaching the smallest diameter grain size, the fraction of HAGBs increases with further straining. An example for the Al-7% Si alloy is shown in Fig. 10 where the elongation to failure increases with the fraction of HAGBs.[123] Secondly, the strain rate sensitivity increases with the imposed strain. The strain rate sensitivity of Cu, for example, increases from ~0.06 to ~0.14 after 16 passes of ECAP[109] and for the Al-7% Si alloy there is an increase from ~0.03 to ~0.14 after 10 turns of HTP.[122] A higher strain rate sensitivity is essential for grain boundary sliding which leads to ductility. In the as-cast Al-7% Si alloy, grain boundary sliding contributes only 1% to the total strain but in the SPD-processed alloy the contribution is ~14%.[123] This shows the increasing importance of grain boundary sliding as a flow process under these experimental conditions. Thirdly, high resolution transmission electron microscopy has provided direct evidence for the presence of non-equilibrium grain boundaries

containing an excess of extrinsic dislocations in alloys processed by SPD[124] and it is reasonable to anticipate that the movement of these extrinsic dislocations permits relatively easy sliding.

In practice, grain boundary siding is generally associated with high temperatures of at least one-half the melting point and an activation energy equal to that for grain boundary diffusion.[125] Nevertheless, there is experimental evidence for grain boundary sliding [GBS] at room temperature. For example, the occurrence of GBS was identified in UFG pure Al processed by ECAP using a depth-sensing indentation technique[126] and there is also a similar report for pure Al using focused ion beam [FIB] milling.[127] Micropillars of an Al-30% Zn alloy were prepared by HPT and FIB milling and tested in compression at room temperature within a depth-sensing ultra-hardness testing machine and this gave a high strain rate sensitivity and direct evidence for the occurrence of GBS.[128] In addition, these experiments showed that the strain avalanches that conventionally occur in the coarse-grained alloy during flow are absent in the UFG material. Furthermore, recent experiments on UFG Pd, a metal with a very high melting point, also showed evidence for GBS at room temperature.[129] For the Al-7% Si alloy discussed earlier, the contribution of GBS to the total strain was as high as ~14% after 5 turns of HPT and ~17% after 10 turns.[123] Further confirmation for the possibility of low temperature GBS in UFG metals comes from diffusion data on pure Ni processed by ECAP which show ultra-fast diffusion at lower temperatures [<400 K (127°C)] with a low activation energy but relaxation of the non-equilibrium grain boundaries at high temperatures [>400 K (127°C)].[130,131]

IV. WEAKENING BY SPD

Contrary to general behavior, some alloys are weakened by ECAP or HPT.[132] For example, when the spray-cast Al-7034 alloy is processed by ECAP at a temperature of 473 K (200°C) the

grain size is reduced from ~2.1 to ~0.3 μm after 6 passes but subsequent tensile testing shows an overall weakening which is attributed to the partial loss during ECAP processing of the hardening metastable η′ phase.[133] An example of this weakening is shown by the results obtained for this alloy in compression testing at room temperature using an initial strain rate of 5.5×10^{-4} s^{-1} where the upper curve in Fig. 11 is for the as-received unprocessed alloy and the lower curves are for samples processed through 1, 2 and 6 passes of ECAP: the designation *Z* direction refers to cutting the samples perpendicular to the flow direction and perpendicular to the upper surface of the ECAP billet.[134] Figure 11 shows also that there is a lower rate of strain hardening after yielding when processing by ECAP.

Weakening also occurs in the Zn-22% Al eutectoid alloy and an example is shown by the hardness measurements in Fig. 12 for samples processed by HPT at room temperature under a pressure of 6.0 GPa with an anvil rotation of 1 rpm.[135] In Fig. 12 the hardness values are plotted against the distance from the center of the disk, the upper broken line corresponds to the unprocessed annealed condition and results are shown for up to a total of 20 turns. It was demonstrated using transmission electron microscopy that rod-shaped precipitates of the stable hcp Zn phase, which are contained within the Al-rich grains in the annealed condition, are absorbed by the Zn-rich grains during processing of the Zn-22% Al eutectoid alloy.[136,137] Similar weakening was also reported in other materials such as the Pb-62% Sn eutectic alloy[138] and the Bi-42% Sn eutectic alloy.[139]

V. SUPERSTRENGTH BY SPD

In addition to a fine grain size, materials processed by SPD may contain additional features such as nanoparticles, nanotwins, non-equilibrium grain boundaries and grain boundary segregation

and the presence of these additional features may permit higher strengths than those predicted by the standard H-P relationship.[140]

For example, Fig. 13 contrasts the YS of Ni after HPT or ECAP and rolling[141] with that of electrodeposited Ni[142-144] shown by the continuous line which corresponds to $\sigma_o \approx 7$ MPa and $k_y \approx 5.7$ MPa.mm$^{1/2}$. For the latter condition, the grains contain no dislocation substructure and normal H-P behavior is observed. The upper dashed line is for UFG Ni processed by HPT or ECAP and subsequent rolling in order to achieve a higher strength. [141] The YS in this case may be calculated by adding the contribution of LAGBs and HAGBs and the non-equilibrium grain boundaries [NGBs] so that[140]

$$\sigma_y = \sigma_o + \sigma_{LAGB} + \sigma_{HAGB} + \sigma_{NGBs} \quad [4]$$

and

$$\sigma_y = \sigma_o + M\ \alpha\ G\ b\ [[1.5\ S_v\ \Theta/\ b]_{LAGB}]^{½} + k_y d^{-1/2} + M\ \alpha\ G\ b\ [\rho_{GBDs}]^{½} \quad [5]$$

where σ_o is the threshold stress, M is the Taylor factor [≈3], α is a constant [~0.24], the term S_v is related to the cell size, Θ is the misorientation angle of the LAGBs and ρ_{GBDs} is the density of the extrinsic grain boundary dislocations. It was shown that the values calculated using this procedure are in good agreement with the experimental results.[140]

The occurrence of superstrength materials led to the observation that there are two critical lengths in the H-P relationship, d_{cr1} and d_{cr2}, as shown in Fig. 14.[145] For UFG materials the H-P exponent may vary from -1/2 to -1 in the region $d_{cr2} < d < d_{cr1}$ and for $d < d_{cr2}$ the value is -3 where this gives a positive slope and exceptional hardening as shown by the upper curve 2. By contrast, the lower curve 1 corresponds to the conventional H-P relationship with the advent of a negative slope or a softening behavior at very small grain sizes.[146,147] Some experimental

evidence is now available for the positive slope at very small grain sizes [148] and generally the strengthening is attributed to the presence of significant grain boundary segregation at grain sizes smaller than ~100 nm.[149,150] This is an area requiring further investigation but generally it is reasonable to anticipate SPD materials will exhibit improved strength and improved functional properties associated not only with their ultrafine grains but also with other nanostructural features that are not generally available in conventional coarse-grained materials.[151]

VI. SUMMARY AND CONCLUSIONS

1. The Hall-Petch relationship is followed over a wide range of grain sizes, including the nanometer range produced by SPD. The slope and intercept values are higher for ultrafine-grained materials produced by SPD than for conventional coarse-grained materials.

2. An increase in strength is generally accompanied by a decrease in ductility. In ultrafine-grained materials it is possible to simultaneously achieve high strength and high ductility [HSHD] by imposing a very high strain in SPD. This is because SPD leads to an increase in the strain rate sensitivity, a higher fraction of high-angle grain boundaries and enhanced grain boundary diffusion. All of these factors favor grain boundary sliding even at relatively low temperatures.

3. A quantitative diagram is available to distinguish HSHD materials based on the normalized strength and normalized elongation. An example is presented for an Al-7% Si alloy. This approach has the advantage that it is possible to characterize all ultrafine-grained materials for HSHD using the same diagram.

4. In some materials, ECAP or HPT may produce weakening even in the presence of grain refinement. At grain sizes below ~50 nm there is also a potential for developing a super-

strength in some materials processed by SPD due to the introduction of nanostructured features such as increased grain boundary segregation.

ACKNOWLEDGEMENTS

We are grateful to Jim Li for decades of friendship and collaboration. NB acknowledges financial support from the organizers for his participation in the TMS J.C.M. Li symposium in Columbus, OH. The work of TGL was supported by the National Science Foundation of the United States under Grant No. DMR-1160966.

REFERENCES

1. H. Gleiter: *Acta Mater*., 2000, vol. 48, pp. 1- 29.

2. T.G. Langdon: *Acta Mater*., 2013, vol. 61, pp. 7035-7059.

3. E.O. Hall: Proc. *Phys. Soc. Lond*. B, 1951, vol. 64, pp. 747-753.

4. N.J. Petch: *J. Iron. Steel Inst.,* 1953, vol. 174, pp. 25-28.

5. Z. Horita, M. Furukawa, M. Nemoto, A.J. Barnes, and T.G. Langdon: *Acta Mater*., 2000, vol. 48, pp. 3633 – 3640.

6. T.G. Langdon: *Mech. Mater*., 2013, vol. 67, pp. 2-8.

7. M. Kawasaki and T.G. Langdon: *J. Mat. Sci*., 2016, vol. 51, pp. 19-32.

8. A.J. Barnes: *J. Mater. Eng. Perform*., 2007, vol. 16, pp. 440 – 454.

9. T.G. Langdon: *Acta Metall. Mater*., 1994, vol. 42, pp. 2437–2443.

10. M. Kawasaki, N. Balasubramanian, and T.G. Langdon: *Mater. Sci. Eng*., 2011, vol. A528, pp. 6624–6629.

10. T.G. Langdon: *Acta Metall. Mater*., 1994, vol. 42, pp. 2437–2443.

11. R.Z. Valiev, D.A. Salimonenko, N.K. Tsenev, P.B. Berbon, and T.G. Langdon: *Scr. Mater*., 1997, vol. 37, pp.1945–1950.

12. R.K. Islamgaliev, N.F. Yunusova, R.Z. Valiev, N.K. Tsenev, V.N. Perevezentsev, and T.G. Langdon: *Scr. Mater*., 2003, vol. 49, pp. 467–472.

13. R. Kaibyshev, K. Shipilova, F. Musin, and Y. Motohashi: *Mater. Sci. Technol*., 2005, vol. 21, pp. 408–418.

14. F. Musin, R. Kaibyshev, Y. Motohashi, and G.Itoh: *Metall. Mater. Trans*., 2004, vol. 35A, pp. 2383–2392.

15. K.T. Park, D.Y. Hwang, Y.K. Lee, Y.K. Kim, and D.H. Shin: *Mater. Sci. Eng*., 2003, vol. A341, pp. 273–281.

16. I. Nikulin, R. Kaibyshev, and T. Sakai: *Mater Sci. Eng*., 2005, vol. A407, pp. 62–70.

17. S. Komura, M. Furukawa, Z. Horita, M. Nemoto, and T.G. Langdon: *Mater Sci*. *Eng*., 2001, vol. A297, pp. 111–118.

18. S. Komura, Z. Horita, M. Furukawa, M.Nemoto, and T.G. Langdon: *Metall. Mater*. *Trans*., 2001, vol. 32A, pp. 707–716.

19. S. Lee, A. Utsunomiya, H. Akamatsu, K. Neishi, M. Furukawa, Z. Horita, and T.G. Langdon: *Acta Mater*., 2005, vol. 50, pp. 553–564.

20. K. Turba, P. Málek, and M. Cieslar: *Mater. Sci. Eng*., 2007, vol. A462, pp. 91–94.

21. R.S. Mishra, R.Z. Valiev, S.X. McFadden, R.K. Islamgaliev, and A.K. Mukherjee: *Philos. Mag*. *A*, 2001, vol. 81, pp.37–48.

22. V.N. Perevezentsev, M.Yu. Shcherban, M.Yu. Murashkin, and R.Z. Valiev: *Tech. Phys. Lett*., 2007, vol. 33, pp. 648–650.

23. S.V. Dobatkin, E.N. Bastarache, G. Sakai, T. Fujita, Z. Horita, and T.G. Langdon: *Mater. Sci. Eng*., 2005, vol. A408, pp. 141–146.

24. A. Alhamidi and Z. Horita: *Mat. Sci. Eng*., 2015, vol. A622, pp. 139-145.

25. C. Xu, S.V. Dobatkin, Z. Horita, and T.G. Langdon: *Mater. Sci., Eng*., 2009, vol. A500, pp. 170–175.

26. S. Sabbaghianrad, M. Kawasaki, and T.G. Langdon: *J. Mater. Sci*., 2012, vol. 47, pp. 7789–7795.

27. M. Kawasaki, J. Foissey, and T.G. Langdon: *Mater. Sci. Eng*., 2013, vol. A561, pp.118–125.

28. G. Sakai, Z. Horita, and T.G. Langdon: *Mater. Sci. Eng*., 2005, vol. A393, pp. 344–351.

29. Y. Harai, K. Edalati, Z. Horita, and T.G. Langdon: *Acta Mater*., 2009, vol. 57, pp. 1147–1153.

30. R.B. Figueiredo and T.G. Langdon: *J. Mater. Sci*., 2008, vol. 43, pp. 7366–7371.

31. Y. Miyahara, Z. Horita, and T.G. Langdon: *Mater. Sci. Eng*, 2006, vol. A420, pp. 240–244.

32. M. Mabuchi, H. Iwasaki, K. Yanase, and K. Higashi: *Scr. Mater*., 1997, vol. 36, pp. 681–686.

33. M. Mabuchi, K. Ameyama, H. Iwasaki, and K. Higashi: *Acta Mater*., 1999, vol. 47, pp. 2047–2057.

34. V.N. Chuvil'deev, T.G. Nieh, M.Yu. Gryaznov, V.I. Kopylov, and A.N. Sysoev: *J*., *Alloys Compd*., 2004, vol. 378, pp. 253–257.

35. K. Yan, Y-S. Sun, J. Bai, and F. Xue: *Mater. Sci. Eng.*, 2011, vol. 528, pp. 1149–1153.

36. H. Watanabe, T. Mukai, K. Ishikawa, and K. Higashi: *Scr. Mater*., 2002, vol. 46, pp. 851–856.

37. V.N. Chuvil'deev, T.G. Nieh, M.Yu. Gryaznov, A.N. Sysoev, and V.I. Kopylov: *Scr. Mater.*, 2004, vol. 50, pp. 861–865.

38. R.B. Figueiredo and T.G. Langdon: *Mater. Sci. Eng*., 2006, vol. A430, pp.151–156.

39. R.B. Figueiredo and T.G. Langdon: *Adv. Eng. Mater*., 2008, vol. 10, pp. 37–40.

40. Y. Miyahara, K. Matsubara, Z. Horita, and T.G. Langdon: *Metall. Mater. Trans.*, 2005, vol. 36A, pp. 1705–1711.

41. K. Matsubara, Y. Miyahara, Z. Horita, and T.G. Langdon: *Acta Mater*. 2003, vol. 51, pp. 3073–3084.

42. M. Furui, C. Xu, T. Aida, M. Inoue, H. Anada, and T.G. Langdon: *Mater. Sci. Eng*., 2005, vol. A410–411, pp. 439–442

43. M. Furui, H. Kitamura, H. Anada, and T.G. Langdon: *Acta Mater*., 2007, vol. 55, pp. 1083–1091.

44. S.W. Xu, M.Y. Zheng, S. Kamado, and K. Wu: *Mater. Sci. Eng*., 2012, vol. A549, pp. 60–68.

45. Z. Kang, L. Zhu, and J. Zhang: *Mater. Sci. Eng*., 2015, vol. A633, pp. 59–62.

46. Y. Harai, M. Kai, K. Kaneko, Z. Horita, and T.G. Langdon: *Mater. Trans*., 2008, vol. 49, pp. 76–83.

47. S.A. Torbati-Sarraf and T.G. Langdon: *J. Alloys Compd*., 2014, vol. 613, pp. 357–363.

48. M. Kai, Z. Horita, and T.G. Langdon: *Mater. Sci. Eng*., 2008, vol. A488, pp. 117– 124.

49. O.B. Kulyasova, R.K. Islamgaliev, A.R. Kil'mametov, and R.Z. Valiev: *Phys. Met. Metallogr*., 2006, vol. 101, pp. 585–590.

50. R.Z. Valiev, R.K. Islamgaliev, and I.V. Alexandrov: *Prog. Mater. Sci*., 2000, vol. 45, pp. 103 -189.

51. R.Z. Valiev, Y. Estrin, Z. Horita, T.G. Langdon, M.J. Zehetbauer, and Y.T. Zhu: *JOM*, 2006, vol. 58, no. 4, pp. 33-39.

52. M. Furukawa, Z. Horita, M. Nemoto, and T.G. Langdon: *J. Mater. Sci*., 2001, vol. 36, pp. 2835 – 2843.

53. R.Z. Valiev and T.G. Langdon: *Prog. Mater. Sci*., 2006, vol. 51, pp. 881- 981.

54. A.P. Zhilyaev and T.G. Langdon: *Prog, Mater. Sci*., 2008,vol. 53, pp. 893-979.

55. M. Ebrahimi, H. Gholipour, and F. Djavanroodi: *Mater. Sci. Eng*., 2015, DOI: 10.1016/j.msea.2015.10.014, on line.

56. Y. Saito, N. Tsuji, H. Utsunomiya, T. Sakai, and R.G. Hong: *Scr. Mater*., 1998, vol. 39, pp. 1221- 1227.

57. K. Lu and J. Lu: *Mater. Sci. Eng.*, 2004, vol. A375-377, pp. 38-45.

58. J.Y. Huang, Y.T. Zhu, J.H. Jiang, and T.C. Lowe: *Acta Mater*., 2001, vol. 49, pp. 1497-1505.

59. C. Xiao, R.A. Mirshams, S.H. Whang, and W.M. Yin: *Mat. Sci. Eng*., 2001, vol. A301, pp. 35–43

60. D.A. Hughes and N. Hansen: *Phys. Rev. Lett*., 2014, vol. 112, p. 135504.

61. J.R. Low, Jr. and M Gensamer: *Trans. TMS-AIME*, 1944, vol. 158, pp. 207-214.

62. A.H. Cottrell and B.A. Bilby: *Proc. Phys. Soc. Lond*. 1949, vol. 62, pp. 49-62.

63. A.H. Cottrell: *Trans. TMS-AIME*, 1958, vol. 212, pp. 192-203.

64. K. Prewo, J.C.M. Li, and M. Gensamer: *Metall. Trans*., 1972, vol. 3, pp. 2262-2269.

65. V.S. Ananthan and E.O. Hall: *Acta Metall. Mater*., 1991, vol. 39, pp. 3153-3160.

66. N. Balasubramanian, J.C.M. Li, and M. Gensamer: *Mater. Sci. Eng*., 1974, vol. 14, pp. 37-45.

67. N. Tsuji, Y. Ito, Y. Saito, and Y. Minamino: *Scr. Mater*., 2002, vol. 47, pp. 893-899.

68. X.H. An, S.D. Wu, Z.F. Zhang, R.B. Figueiredo, N. Gao, and T.G. Langdon: *Scr. Mater*., 2012, vol. 66, pp. 227-230.

69. M. Joshi, Y. Fukuta, S. Gao, N. Park, D. Terada and N. Tsuji: IOP Conf. Series: *Mater. Sci. Eng*., 2014, vol. 63, p. 012074.

70. D. Terada, M. Inoue, H. Kitahara, and N. Tsuji: *Mater. Trans*., 2008, vol. 49, pp. 41-46.

71. Z. Li, L. Fu, B. Fu, and A. Shan: *Mater. Lett*., 2013, vol. 96, pp. 1- 4.

72. I. Sabirov, Y. Estrin, M.R. Barnett, I. Timokhina, and P.D. Hodgson: *Acta Mater*., 2008 vol. 56, pp. 2223-2230.

73. R. Saha, R. Ueji, and N. Tsuji: *Scr. Mater*., 2013, vol. 68. pp. 813-816.

74. R.W. Armstrong: *Metall. Trans*., 2015, DOI: 10.1007/s11661-015-3161-4, on line.

75. D.H. Lee, I.C. Choi, M.Y. Seok, J. He. Z. Lu, J.Y. Suh, M. Kawasaki, T.G. Langdon, and J.I. Jang: *J. Mater. Res*., 2015, vol. 30, pp. 2804-2815.

76. A.V. Sergueeva, V.V. Stolyarov, R.Z. Valiev, and A.K. Mukherjee: *Scr. Metall*., 2001, vol. 45, pp. 747-752.

77. V.V. Stolyarov, Y.T. Zhu, I.V. Alexandrov, T.C. Lowe, and R.Z. Valiev: *Mater. Sci*. *Eng*., 2001, vol. A299, pp. 59- 67.

78. V.V. Stolyarov, Y.T. Zhu, T.C. Lowe, R.K. Islamgaliev, and R.Z. Valiev: *Mater*. *Sci. Eng*., 2001, vol. 303, pp. 82-89.

79. D.A. Konstantinidis and E.C. Aifantis: *Nanostruct. Mater*., 1998, vol. 10, pp. 1111- 1118.

80. G.A. Salishchev, R.M. Galeyev, S.P. Malysheva, and M.M. Myshlyaev: *Nanostruct*. *Mater*., 1999, vol. 11, pp. 407- 414.

81. C. T. Wang, N. Gao, M.G. Gee, R.J.K. Wood, and T.G. Langdon: *J. Mater. Sci*., 2013, vol. 48, pp. 4742–4748.

82. X. Zhao, W. Fu, X. Yang, and T.G. Langdon: *Scr. Mater*., 2008, vol. 59, pp. 542 – 545.

83. X. Zhao, X. Yang, X. Liu, X. Wang, and T.G. Langdon: *Mater. Sci. Eng*., 2010, vol. A527, pp. 6335 – 6339.

84. Y.G. Ko, D.H. Shin, K.T. Park, and C.S. Lee: *Scr. Mater*., 2006, vol. 54, pp. 1785- 1789.

85. G.G. Yapici, I. Karaman, and H.J. Maier: *Mater. Sci. Eng*., 2006, vol. A434, pp. 294- 302.

86. V.V. Stolyarov, L. Zeipper, B. Mingler, and M. Zehetbauer: *Mater. Sci. Eng*., 2008, vol. A476, pp. 98 – 105.

87. D.H. Kang and T.W. Kim: *Mater. Des*., 2010, vol. 31, pp. 554- 560.

88. I. Sabirov, R.Z. Valiev, I.P. Semenova, and R. Pippan: *Metall. Mater. Trans*., 2010, vol. 41A, pp. 727–733.

89. G. Purcek, G.G. Yapici, I. Karaman, and H.J. Maier: *Mater. Sci. Eng*,, 2011, vol. A528, pp. 2303- 2308.

90. Y. Zhang, R.B. Figueiredo, S.N. Alhajeri, J.T. Wang, N. Gao, and T.G. Langdon: *Mater. Sci. Eng*., 2011, vol. A528, pp. 7708 – 7714.

91. V.L. Sordi, M. Ferrante, M. Kawasaki, and T.G. Langdon: *J. Mater. Sci*., 2012, vol. 47, pp. 7870 – 7876.

92. C.T. Wang, N. Gao, M.G. Gee, R.J.K. Wood, and T.G. Langdon: *Wear*, 2012, vol. 280, pp. 28-36.

93. V.V. Stolyarov, Y.T. Zhu, T.C. Lowe, R.K. Islamgaliev, and R.Z. Valiev: *Nanostruct. Mater*., 1999, vol. 11, pp. 947 – 954.

94. A.V. Sergueeva, V.V. Stolyarov, R.Z. Valiev, and A.K. Mukherjee: *Scr. Mater*., 2001, vol. 45, pp. 747 – 752.

95. V.V. Stolyarov, Y.T. Zhu, I.V. Alexandrov, T.C. Lowe, and R.Z. Valiev: *Mater. Sci. Eng*., 2001, vol. A299, pp. 59-67.

96. V.V. Stolyarov, Y.T. Zhu, T.C. Lowe, and R.Z. Valiev: *Mater. Sci. Eng*., 2001, vol. A303, pp. 82 – 89.

97. V.V. Stolyarov, Y.T. Zhu, I.V. Alexandrov, T.C. Lowe, and R.Z. Valiev: *Mater. Sci. Eng*., vol. A343, pp. 43-50.

98. I.P. Semenova, R.Z. Valiev, E.B. Yakushina, G.H. Salimgareeva, and T.C. Lowe: *J. Mater. Sci*., 2008, vol. 43, pp. 7354-7359.

99. R.K. Islamgaliev, V.U. Kazyhanov, L.O. Shestakova, A.V. Sharafutdinov, and R.Z. Valiev: *Mater. Sci. Eng*, 2008, vol. 493, pp. 190-194.

100. G. Purcek, O. Saray, O. Kul, I. Karaman, G.G. Yapici, M. Haouaoui, and H.J. Maier: *Mater. Sci. Eng*., 2009, vol. A517, pp. 97-104.

101. S. Faghihi, D. Li, and J.A. Szpunar: *Nanotechnol*., 2010, vol. 21, p. 485703.

102. P. Luo, D.T. McDonald, W.Xu, S. Palanisamy, M.S. Dargusch, and K. Xia: *Scr*. *Mater*. vol. 66, pp. 785-788.

103. P. Bazarnik, Y. Huang, M. Lewandowska, and T.G. Langdon: *Mater. Sci. Eng*., 2015, vol. A626, pp. 9-15.

104. N. Hansen: *Scr. Mater*., 2004, vol. 51, pp. 801-806.

105. M. Furukawa, Z. Horita, M. Nemoto, R.Z. Valiev, and T.G. Langdon: *Philos. Mag*. *A* 1998, vol. 78, pp. 203-215.

106. M. Furukawa, Z. Horita, M. Nemoto, R.Z. Valiev, and T.G. Langdon : *Acta Met*. 1996, vol. 44, pp. 4619-4629.

107. N. Tsuji: in Nanostructured Materials by High Pressure Severe Plastic Deformation, ed. Y.T. Zhu and V. Varyukhin. 2006, Springer, Netherlands, pp. 227-234.

108. R.Z. Valiev: *Nature*, 2011, vol. 419, pp. 887-889.

109. R.Z. Valiev, I.V. Alexandraov, Y.T. Zhu, and T.C. Lowe: *J. Mater. Res*., 2002, vol. 17, pp. 5-8.

110. T. Suo, Y. Li, F. Zhao, Q. Deng, and K. Xie: *Mater. Res. Innov*. 2011, vol. 15, pp. 69-72

111. I. Semenova, G. Salimgareeva, G. Da Costa, W. Lefebvre, and R. Z. Valiev: *Adv*. *Eng. Mater*., 2010, vol.12, pp. 803-807

112. A.V. Polykov, I. P. Semenova, R. Z. Valiev, Y. Huang, and T.G. Langdon: *MRS Comm*. 2013, vol. 3, pp. 249-253.

113. N. Maury, N.X. Zhang, Y. Huang, A.P. Zhilyaev, and T.G. Langdon: *Mater. Sci. Eng*., vol. A638, pp. 174-182.

114. O. Andreau, J. Gubicza, N.X. Zhang, Y. Huang, P. Jenei, and T.G. Langdon: *Mater. Sci. Eng*., 2014, vol. A615, pp. 231-239.

115. K. Edalati, T. Furuta, T. Daio, S. Kuramoto, and Z. Horita: *Mater. Res. Lett*., 2015, vol. 3, pp. 197-202.

116. L. Lu, Y.F. Shen, X.H. Chen, L.H. Qian, and K. Lu: *Science*, 2004. vol. 304, pp. 422-426.

117. K. Edalati, S.Toh, T. Furuta, S. Kuramoto, M. Watanabe, and Z. Horita: *Scr. Mater*. 2012, vol. 67, pp. 511-51.

118. Y. Wang, M. Chen, F. Zhou, and E. Ma: *Nature*, 2002, vol. 419, pp. 912-915.

119. Y. Waseda, S. Ueno, M. Hagiwara, and K.T. Aust: *Prog. Mater. Sci*., 1990, vol. 34, pp. 149-260.

120. S. Pauly, S. Gorantla, G. Wang, U. Kuhn, and J. Eckert: *Nature Mater*. 2010, vol. 9, pp. 473-477.

121. P. Kumar, M. Kawasaki, and T.G. Langdon: *J. Mater. Sci*., 2016, vol. 51, pp. 7-18.

122. T. Mungole, P. Kumar, M. Kawasaki, and T.G. Langdon: *J. Mater. Res*., 2014, vol. 29, pp. 2534-2546.

123. T. Mungole, P. Kumar, M. Kawasaki and T.G. Langdon: *J. Mater. Sci*., 2015, vol. 50, pp. 3549-3561.

124. Z. Horita, D.J. Smith, M. Furukawa, M. Nemoto, R.Z. Valiev, and T.G. Langdon: *J. Mater. Res*. 1996, vol. 11, p. 1880-1890.

125. R.C. Gifkins and T.G. Langdon: *J. Inst. Metals*, 1965, vol. 93, pp. 1347-1352.

126. N.Q. Chinh, P. Szommer, Z. Horita, and T.G. Langdon: *Adv. Mater*., 2006, vol. 18, pp. 34 - 39.

127. K.V. Ivanov and E.V. Naydenkin: *Mater. Sci. Eng*., 2014, vol. A606, pp. 313-321.

128. N.Q. Chinh, T. Györi, R.Z. Valiev, P. Szommer, G. Varga, K. Havancsák, and T.G. Langdon: *MRS Comm*., 2012, vol. 2, pp. 75-78.

129. K. Yang, H.J. Fecht, and Y. Ivanisenko: *Adv. Eng. Mater*., 2014, vol. 16, pp. 517-521.

130. S.V. Divinski, G. Reglitz, H. Rösner, Y. Estrin, and G. Wilde: *Acta Mater*., 2011, vol. 59, pp. 1974-1985.

131. S.V. Divinski, G. Reglitz, I.S. Golovin, M. Peterlechner, R. Lopovok, Y. Estrin, and G. Wilde: *Acta Mater*., 2015, vol. 82, pp. 11-21.

132. T. G. Langdon: *Kovove Mater*., 2015, vol. 53, pp. 1-7.

133. C. Xu, M. Furukawa, Z. Horita, and T.G. Langdon: *Acta Mater*. 2005, vol. 53, pp. 749-758.

134. C. Xu, Z. Száraz, Z. Trojanová, P. Lukáč, and T.G. Langdon: *Mater. Sci. Eng*., 2008, vol. A497, pp. 206-211.

135. T.S. Cho, H.J. Li, B. Ahn, M. Kawasaki, and T.G. Langdon: *Acta. Mater*., 2014, vol. 72, pp. 67-79.

136. M. Furukawa, Z. Horita, M. Nemoto, R.Z. Valiev, and T.G. Langdon: *J. Mater. Res*. 1996, vol. 11, pp. 2128-2130.

137. M. Furukawa, Z. Horita, M. Nemoto, R.Z. Valiev, and T.G. Langdon: *Mater. Sci. Eng*., 1998. vol. A241, pp. 122-128.

138. N.X. Zhang, M. Kawasaki, Y. Huang, and T.G. Langdon: *J. Mater. Sci*., 2013, vol. 48, pp. 4582-4591.

139. C.T. Wang and T.G. Langdon: IOP Conf. Series: *Mater. Sci. Eng*., 2014, vol. 63, p. 012107.

140. R.Z. Valiev, N.A. Enikeev, and T.G. Langdon: *Kovove Mater*. 2011, vol. 49, pp. 1-9.

141. N. Krasilnikov, W. Lojkowski, Z. Pakiela, and R.Z. Valiev: *Mat. Sci. Eng*. , 2005, vol. A397, pp. 330-337.

142. C. Xiao, R.A. Mirshams, S.H. Whang, and W.M. Yin: *Mat. Sci. Eng.*, 2001, vol. A301, pp. 35–43.

143. A.W. Thompson: *Acta Metall*., 1975, vol. 23, pp. 1337-1342.

144. F. Ebrahimi, G.R. Bourne, M.S. Kelly, and T.E. Matthews: *Nanostruct. Mater*., 1999, vol. pp. 343-350.

145. S.A. Firstov, T.G. Rogul, and O.A. Shut: *Functional Mater*., 2009, vol. 16, pp. 364-373.

146. A. Chokshi, A. Rosen, J. Karch, and H. Gleiter: *Scri. Metall*. 1989, vol. 23, pp. 1679-1684.

147. H. Conrad and J. Narayan: *Scri. Mater*., 2000, vol. 42, pp. 1025-1030.

148. R.Z. Valiev: *Mater. Trans*., 2014, vol. 55, pp. 13-18.

149. R.Z. Valiev, N.A. Enikeev, M.Yu. Murashkin, V.U. Kazykhanov, and X. Sauvage: 2010, *Scri. Mater*., vol. 63, pp. 949-952.

150. X. Sauvage, G. Wilde, S.V. Divinski, Z. Horita, and R.Z. Valiev: *Mater. Sci. Eng*., 2012, vol. A540, pp. 1-12.

151. R.Z. Valiev, Y. Estrin, Z. Horita, T.G. Langdon, M.J. Zehetbauer, and Y.T. Zhu: *Mater. Res. Lett*., 2016 http://dx.doi.org/10.1080/21663831.2015.1060543 , on line.

FIGURE CAPTIONS

Figure. 1a. Effect of grain size on superplastic strain rate in Al alloys;[7] datum points for ECAP [11-20] are in black and for HPT [21-29] in red; the encircling ovals are in blue for ECAP and pink for HPT and the solid line corresponds to eq. (2) in the text.

Figure. 1b. Effect of grain size on superplastic strain rate in Mg alloys;[7] datum points for ECAP [30-45] and HPT. [46-49]

Figure 2. Microhardness-grain size relation in commercial purity Ti;[76] the H-P relationship holds down to 9 nm using experimental data.[76,80]

Figure 3. The H-P relationship for Ti;[81] grades 1 to 4 denote increasing orders of impurities for Fe, N and O and using experimental data.[81-100]

Figure 4. The H-P relationship for coarse- grained and HPT processed Al-5% Mg;[103] with increasing numbers of turns, HAGBs develop and the H-P relationship is followed so that data from coarse grain samples fall on the same line as HPT specimens.

Figure 5. The strength ductility relation;[109] high strength is generally accompanied by low ductility [shaded region] but, exceptionally, ultrafine–grain Ti and Ni have high strength and high ductility.

Figure 6. Strength vs. ductility for Fe-Ni-Al-C alloy; [115] data for amorphous alloys [119,120], nanotwins [116], bimodal structure [118] and lattice softening and nanotwins [117] are also included.

Figure 7. Strength and ductility presented in a quantitative form as normalized yield stress vs. normalized elongation;[121] materials in the upper open area have gained both high strength and high ductility as a result of processing.

Figure 8. Stress-strain diagram for Al-7% Si alloy showing the increase in strength and ductility due to HPT and tensile testing at 298 K (25°C).[122]

Figure 9. The improvement in the Al-7% Si alloy due to HPT plotted on the quantitative diagram shown in Fig. 7; points in the upper region exhibit both high strength and high ductility.[122]

Figure 10. Elongation to failure correlated with the fraction of HAGBs measured in an Al-7% Si alloy processed by HPT. [121]

Figure 11. Stress-strain curves for Al–7034 showing the weakening through increasing numbers of ECAP passes.[134]

Figure 12. Weakening in Zn-22% Al with increasing numbers of HPT turns.[135]

Figure 13. Superstrength in Ni subjected to ECAP and subsequent rolling;[140] the dashed line shows UFG Ni [141] and the solid line shows H-P behavior in nano-Ni fabricated by electroplating. [142-144]

Figure 14. Schematic illustration of the H-P relationship in superstrong and conventional materials. [145]

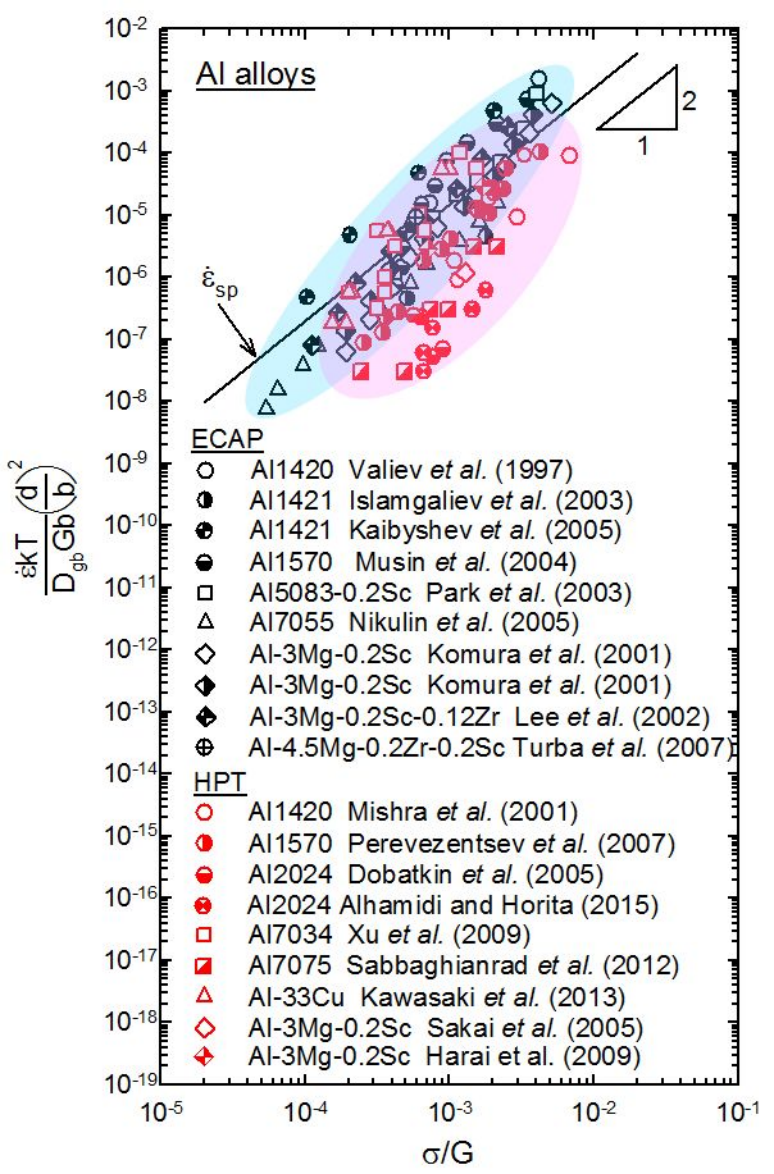
Al alloys
2
1
$\dot{\varepsilon}_{sp}$
ECAP
Al1420 Valiev et al. (1997)
Al1421 Islamgaliev et al. (2003)
Al1421 Kaibyshev et al. (2005)
Al1570 Musin et al. (2004)
Al5083-0.2Sc Park et al. (2003)
Al7055 Nikulin et al. (2005)
Al-3Mg-0.2Sc Komura et al. (2001)
Al-3Mg-0.2Sc Komura et al. (2001)
Al-3Mg-0.2Sc-0.12Zr Lee et al. (2002)
Al-4.5Mg-0.2Zr-0.2Sc Turba et al. (2007)
HPT
Al1420 Mishra et al. (2001)
Al1570 Perevezentsev et al. (2007)
Al2024 Dobatkin et al. (2005)
Al2024 Alhamidi and Horita (2015)
Al7034 Xu et al. (2009)
Al7075 Sabbaghianrad et al. (2012)
Al-33Cu Kawasaki et al. (2013)
Al-3Mg-0.2Sc Sakai et al. (2005)
Al-3Mg-0.2Sc Harai et al. (2009)
$\frac{\dot{\varepsilon}kT}{D_{gb}Gb}\left(\frac{d}{b}\right)^2$
σ/G
10^{-2}
10^{-3}
10^{-4}
10^{-5}
10^{-6}
10^{-7}
10^{-8}
10^{-9}
10^{-10}
10^{-11}
10^{-12}
10^{-13}
10^{-14}
10^{-15}
10^{-16}
10^{-17}
10^{-18}
10^{-19}
10^{-5}
10^{-4}
10^{-3}
10^{-2}
10^{-1}

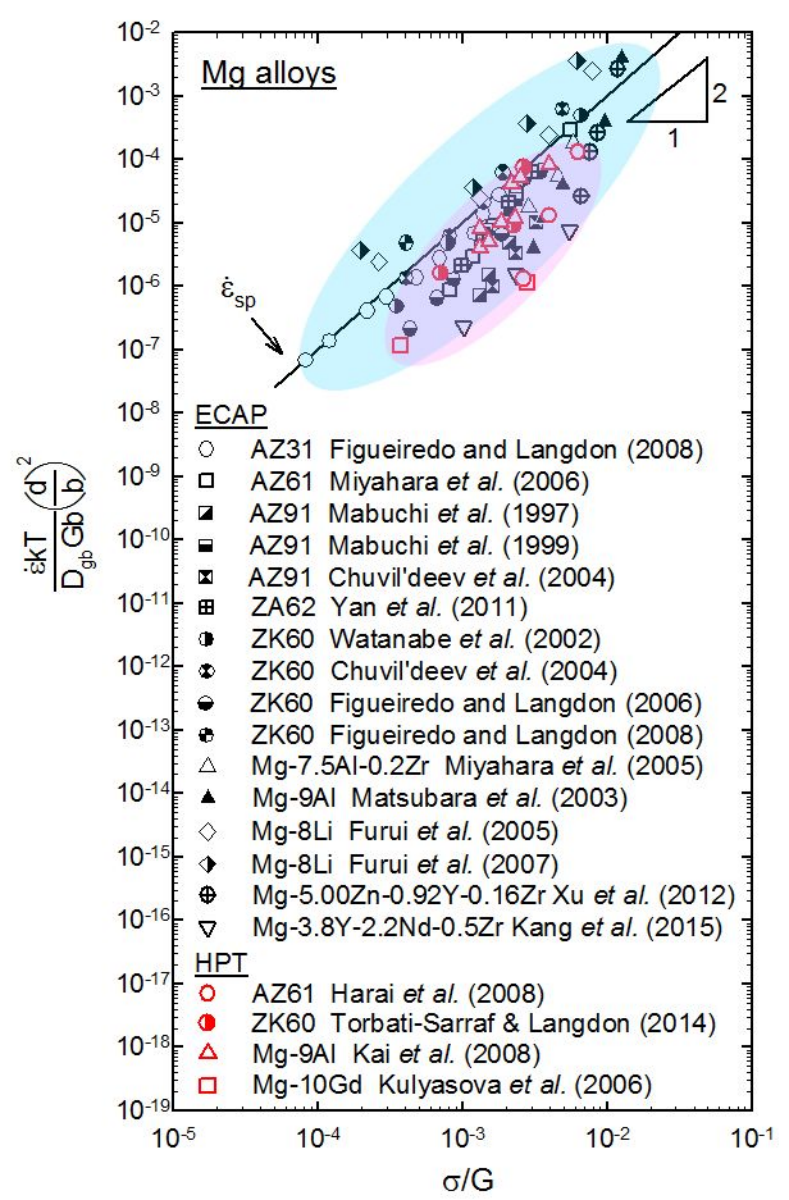
Mg alloys
2
1
$\dot{\varepsilon}_{sp}$
ECAP
AZ31 Figueiredo and Langdon (2008)
AZ61 Miyahara *et al.* (2006)
AZ91 Mabuchi *et al.* (1997)
AZ91 Mabuchi *et al.* (1999)
AZ91 Chuvil'deev *et al.* (2004)
ZA62 Yan *et al.* (2011)
ZK60 Watanabe *et al.* (2002)
ZK60 Chuvil'deev *et al.* (2004)
ZK60 Figueiredo and Langdon (2006)
ZK60 Figueiredo and Langdon (2008)
Mg-7.5Al-0.2Zr Miyahara *et al.* (2005)
Mg-9Al Matsubara *et al.* (2003)
Mg-8Li Furui *et al.* (2005)
Mg-8Li Furui *et al.* (2007)
Mg-5.00Zn-0.92Y-0.16Zr Xu *et al.* (2012)
Mg-3.8Y-2.2Nd-0.5Zr Kang *et al.* (2015)
HPT
AZ61 Harai *et al.* (2008)
ZK60 Torbati-Sarraf & Langdon (2014)
Mg-9Al Kai *et al.* (2008)
Mg-10Gd Kulyasova *et al.* (2006)
$\frac{\dot{\varepsilon}kT}{D_{gb}Gb}\left(\frac{d}{b}\right)^2$
σ/G
10^{-2}
10^{-3}
10^{-4}
10^{-5}
10^{-6}
10^{-7}
10^{-8}
10^{-9}
10^{-10}
10^{-11}
10^{-12}
10^{-13}
10^{-14}
10^{-15}
10^{-16}
10^{-17}
10^{-18}
10^{-19}
10^{-5}
10^{-4}
10^{-3}
10^{-2}
10^{-1}

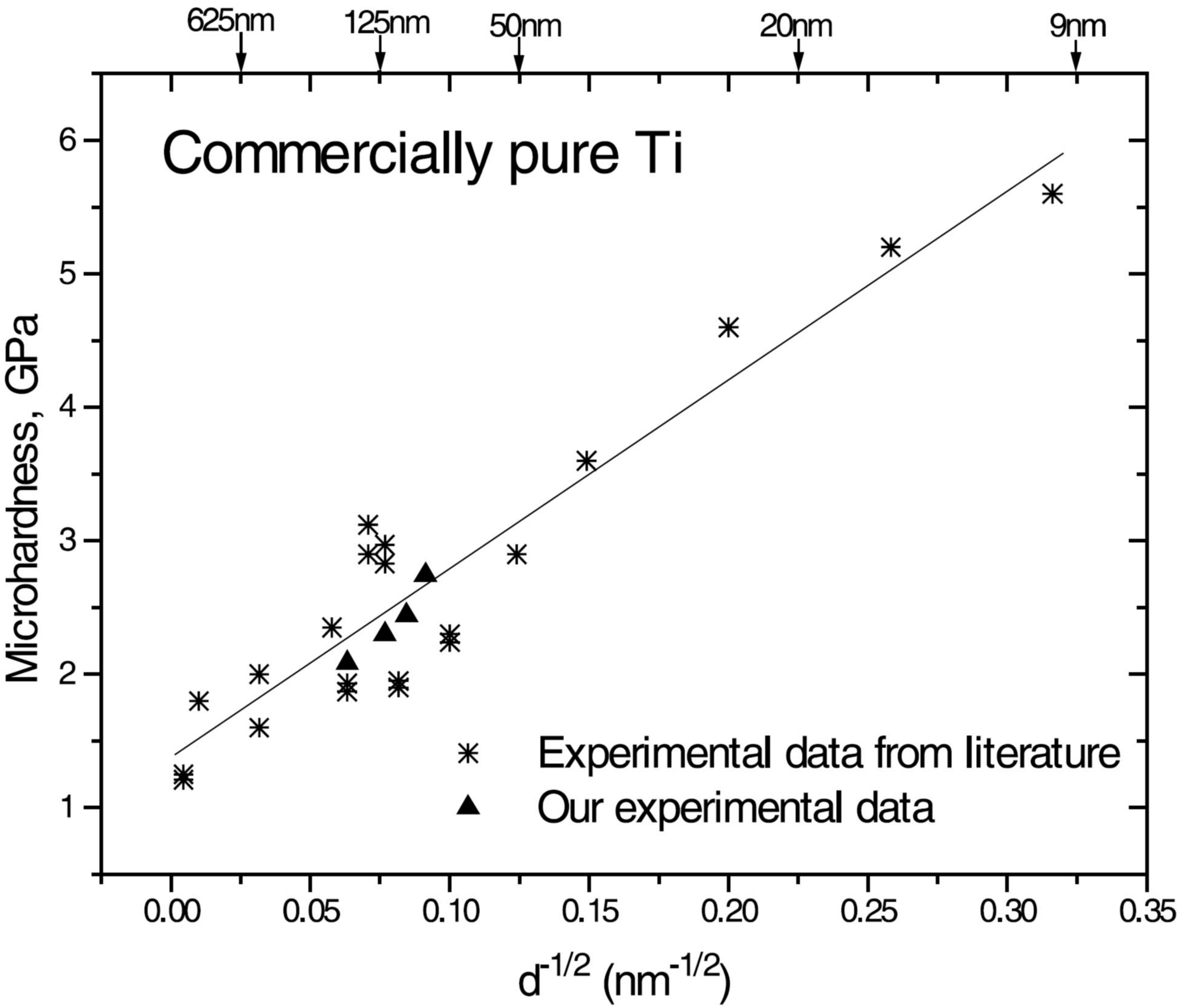
625nm
125nm
50nm
20nm
9nm
Commercially pure Ti
Microhardness, GPa
1
2
3
4
5
6
0.00
0.05
0.10
0.15
0.20
0.25
0.30
0.35
d-1/2 (nm-1/2)
Experimental data from literature
Our experimental data

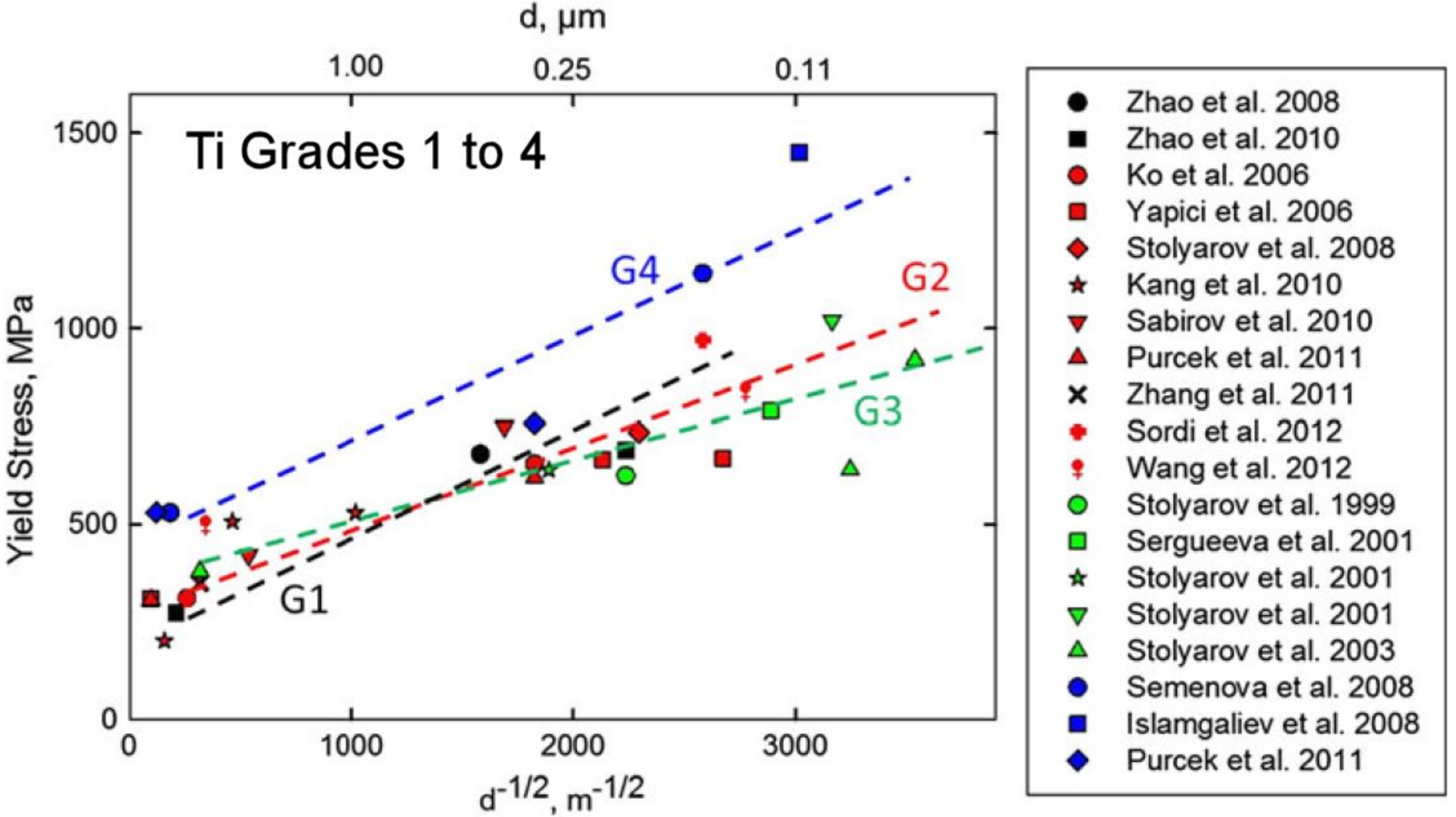
d, μm
1.00
0.25
0.11
Ti Grades 1 to 4
Yield Stress, MPa
1500
1000
500
0
0
1000
2000
3000
d^-1/2, m^-1/2
G1
G2
G3
G4
Zhao et al. 2008
Zhao et al. 2010
Ko et al. 2006
Yapici et al. 2006
Stolyarov et al. 2008
Kang et al. 2010
Sabirov et al. 2010
Purcek et al. 2011
Zhang et al. 2011
Sordi et al. 2012
Wang et al. 2012
Stolyarov et al. 1999
Sergueeva et al. 2001
Stolyarov et al. 2001
Stolyarov et al. 2001
Stolyarov et al. 2003
Semenova et al. 2008
Islamgaliev et al. 2008
Purcek et al. 2011

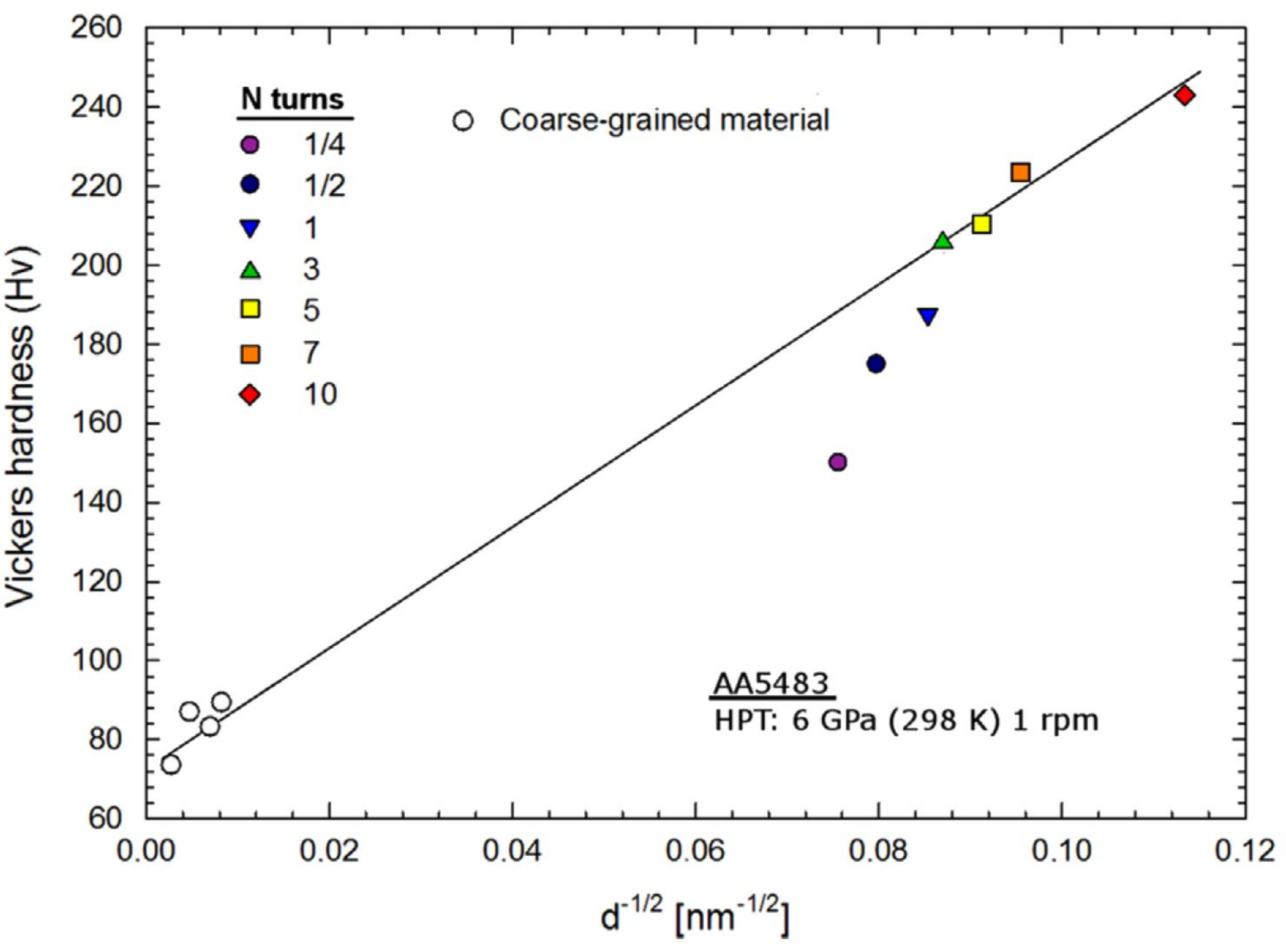
N turns
1/4
1/2
1
3
5
7
10
Coarse-grained material
AA5483
HPT: 6 GPa (298 K) 1 rpm
Vickers hardness (Hv)
d-1/2 [nm-1/2]
260
240
220
200
180
160
140
120
100
80
60
0.00
0.02
0.04
0.06
0.08
0.10
0.12

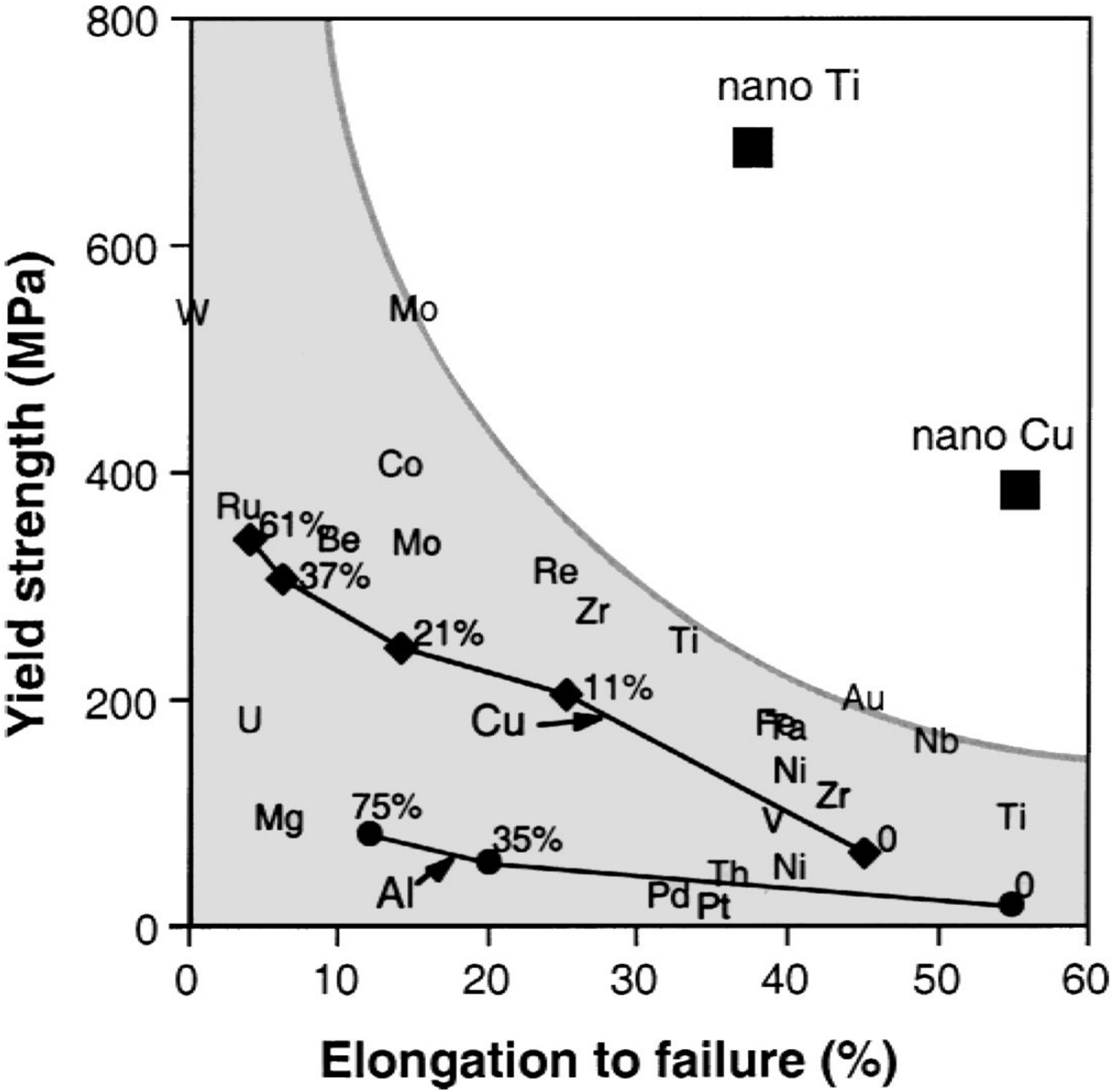
Yield strength (MPa)
800
600
400
200
0
0
10
20
30
40
50
60
Elongation to failure (%)
nano Ti
nano Cu
W
Mo
Co
Ru
61%
Be
Mo
37%
Re
Zr
21%
Ti
11%
Au
U
Cu
Nb
Ni
Zr
Mg
75%
V
Ti
35%
0
Th
Ni
Al
Pd
Pt
0

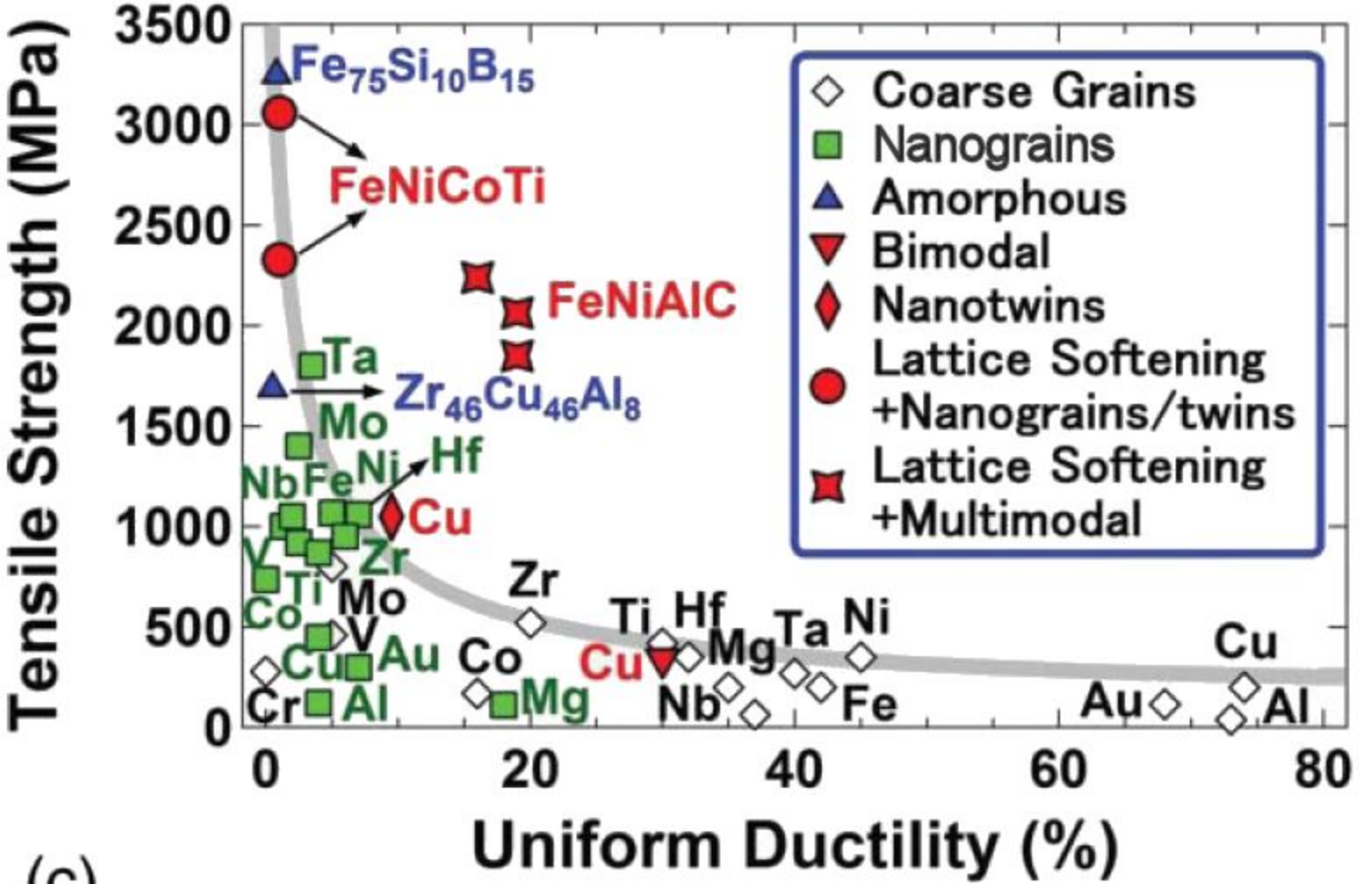
Tensile Strength (MPa)
3500
3000
2500
2000
1500
1000
500
0
0
20
40
60
80
Uniform Ductility (%)
Coarse Grains
Nanograins
Amorphous
Bimodal
Nanotwins
Lattice Softening +Nanograins/twins
Lattice Softening +Multimodal
Fe75Si10B15
FeNiCoTi
FeNiAlC
Zr46Cu46Al8
Ta
Mo
Nb
Fe
Ni
Hf
Cu
V
Zr
Ti
Mo
Co
V
Cu
Au
Cr
Al
Co
Mg
Zr
Ti
Hf
Mg
Ta
Ni
Cu
Nb
Fe
Au
Cu
Al

(c)

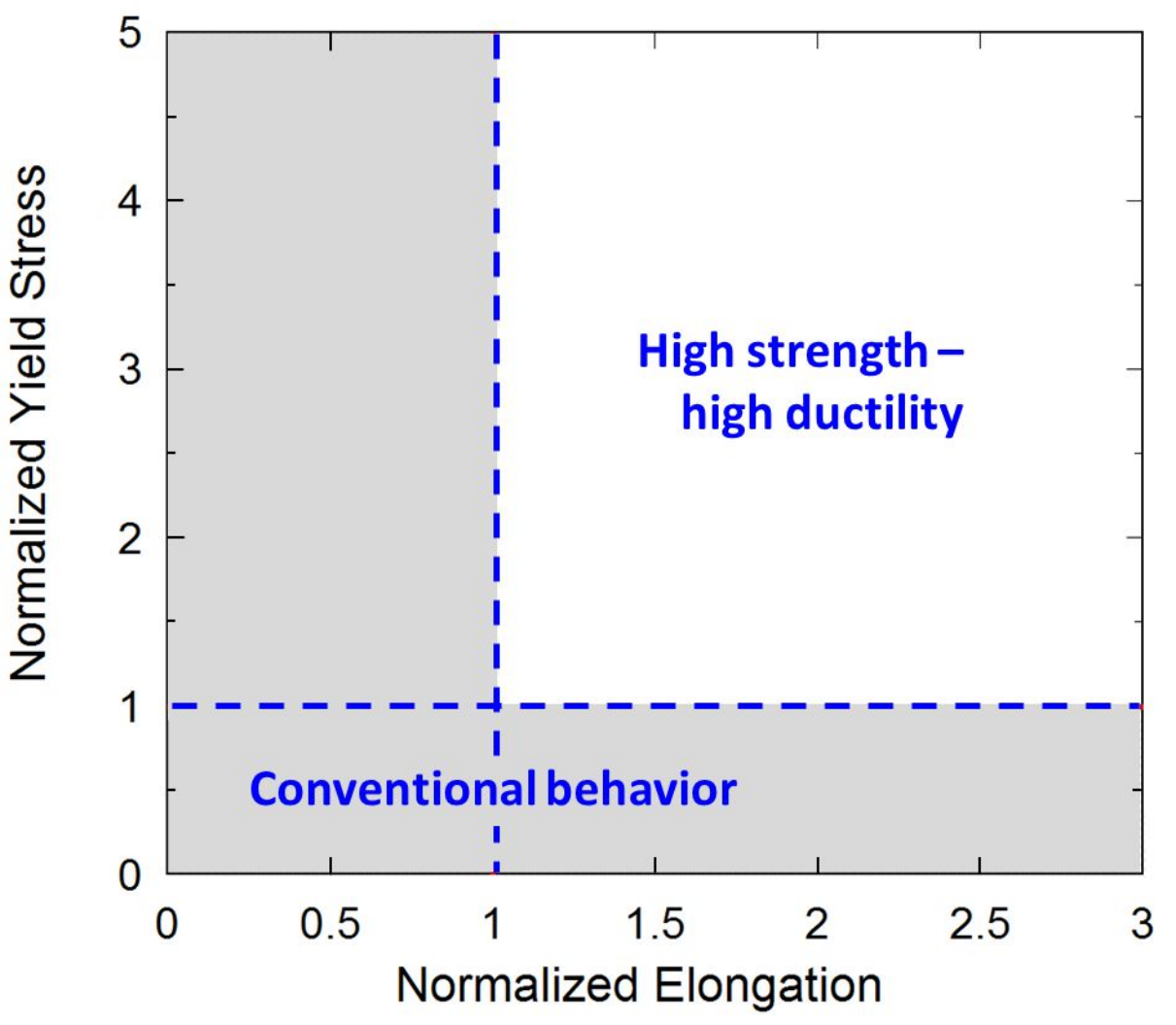
Normalized Yield Stress
Normalized Elongation
High strength –
high ductility
Conventional behavior
0
1
2
3
4
5
0
0.5
1
1.5
2
2.5
3

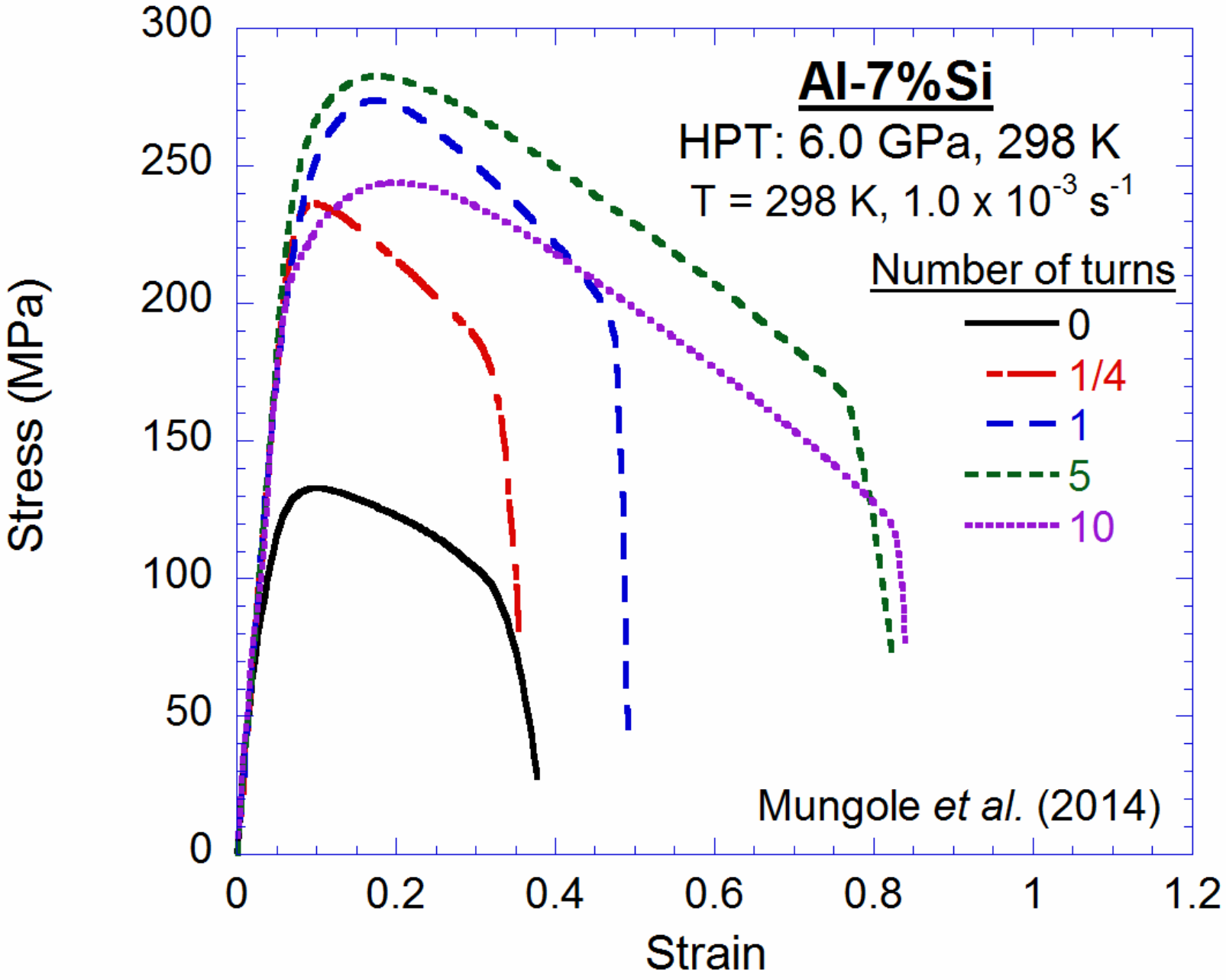
Al-7%Si
HPT: 6.0 GPa, 298 K
T = 298 K, 1.0 x 10^-3 s^-1
Number of turns
0
1/4
1
5
10
Mungole et al. (2014)
Stress (MPa)
Strain
300
250
200
150
100
50
0
0
0.2
0.4
0.6
0.8
1
1.2

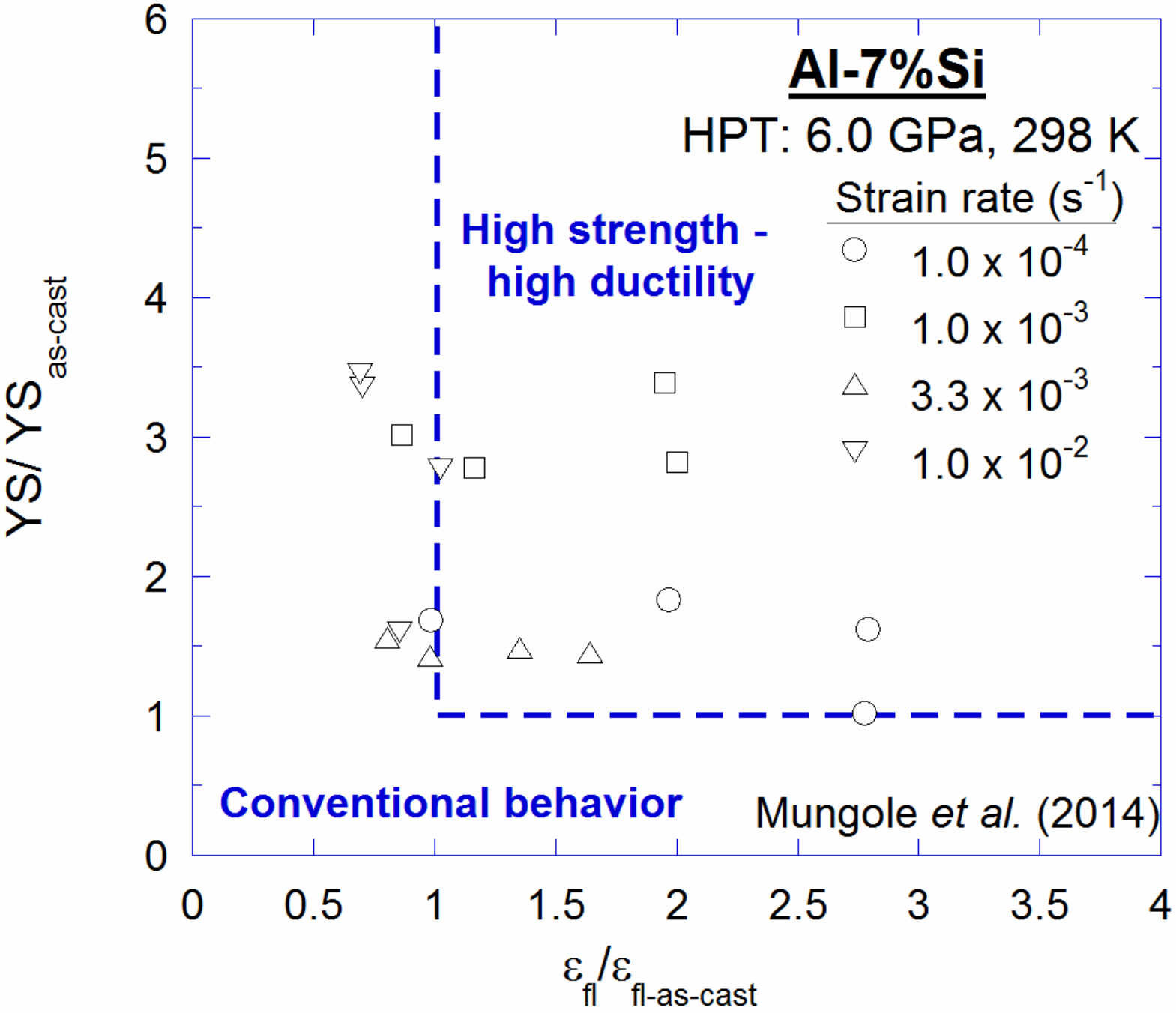
Al-7%Si
HPT: 6.0 GPa, 298 K
Strain rate (s^{-1})
1.0 x 10^{-4}
1.0 x 10^{-3}
3.3 x 10^{-3}
1.0 x 10^{-2}
High strength - high ductility
Conventional behavior
Mungole *et al.* (2014)
YS/ $YS_{as-cast}$
$\varepsilon_{fl}/\varepsilon_{fl\text{-}as\text{-}cast}$
0
1
2
3
4
5
6
0
0.5
1
1.5
2
2.5
3
3.5
4

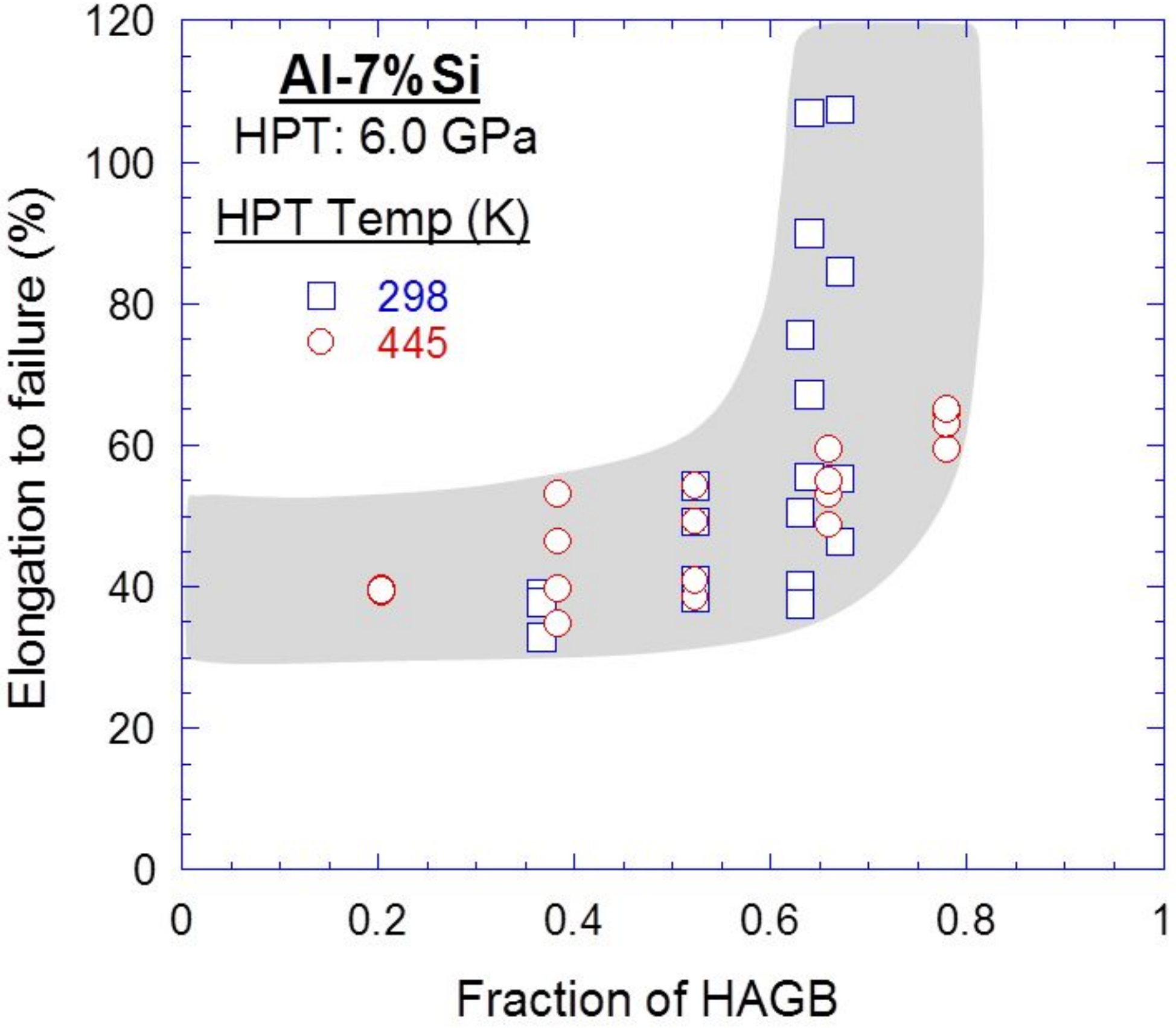
Al-7% Si
HPT: 6.0 GPa
HPT Temp (K)
298
445
Elongation to failure (%)
Fraction of HAGB
120
100
80
60
40
20
0
0
0.2
0.4
0.6
0.8
1

Al-6061 (Z direction)

T = 298 K

$\dot{\varepsilon} = 5.5 \times 10^{-4}\ s^{-1}$

ECAP: 6p

ECAP: 2p

ECAP: 1p

As-received

Engineering stress (MPa)

Engineering strain (%)

0
100
200
300
400
500

0
5
10
15
20
25
30
35

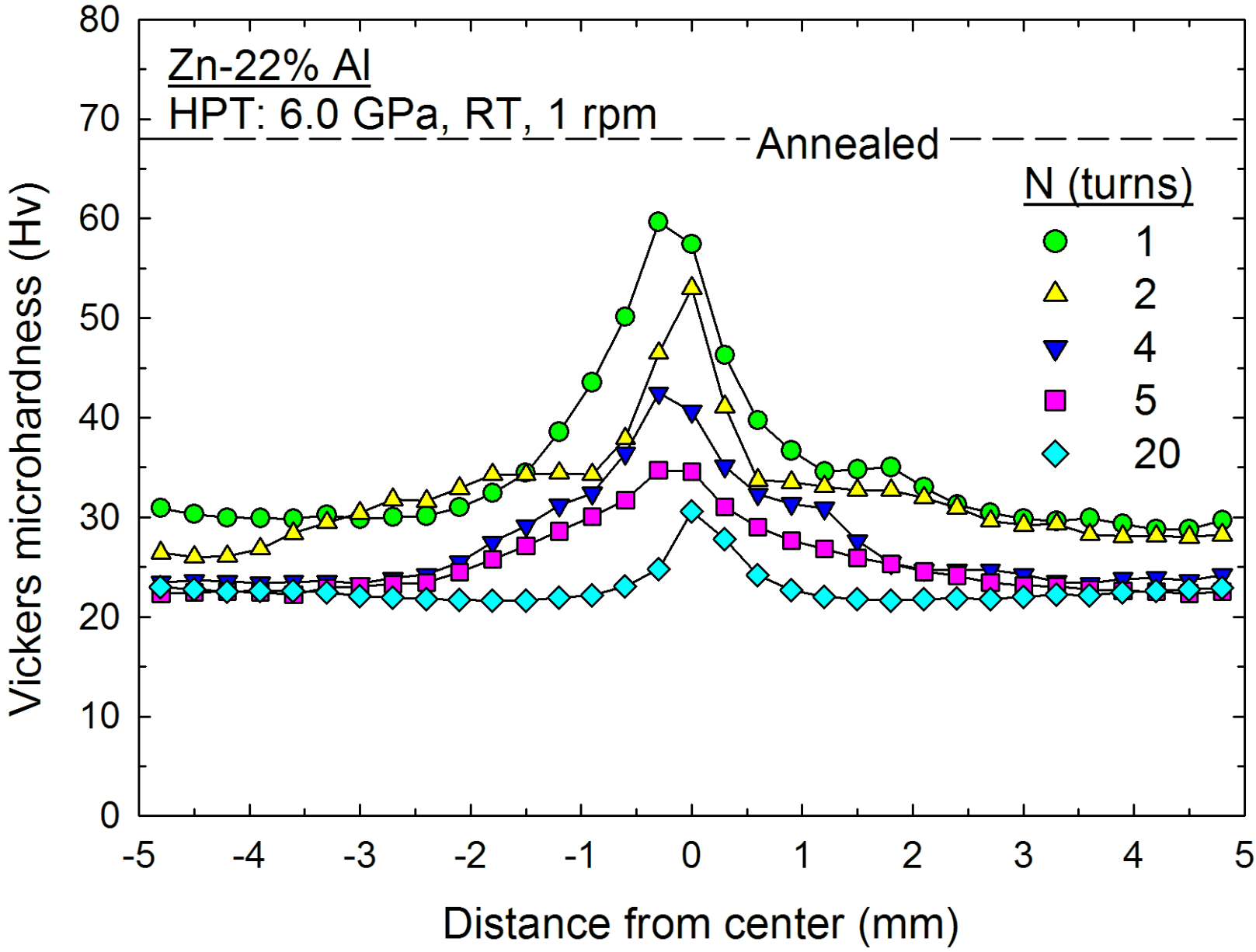
Zn-22% Al
HPT: 6.0 GPa, RT, 1 rpm
Annealed
N (turns)
1
2
4
5
20
Vickers microhardness (Hv)
Distance from center (mm)
0
10
20
30
40
50
60
70
80
-5
-4
-3
-2
-1
0
1
2
3
4
5

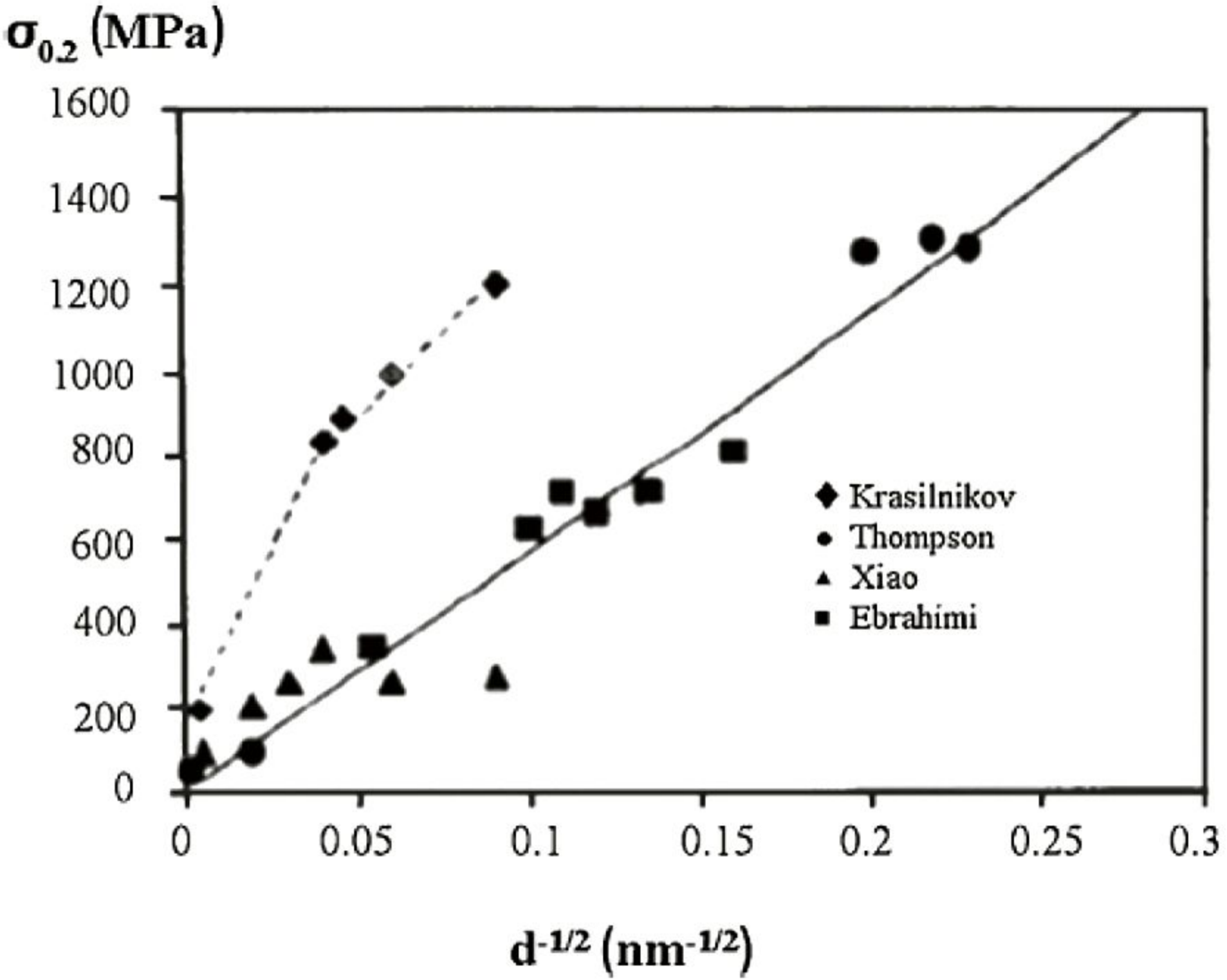
σ0.2 (MPa)
1600
1400
1200
1000
800
600
400
200
0
0
0.05
0.1
0.15
0.2
0.25
0.3
d-1/2 (nm-1/2)
Krasilnikov
Thompson
Xiao
Ebrahimi

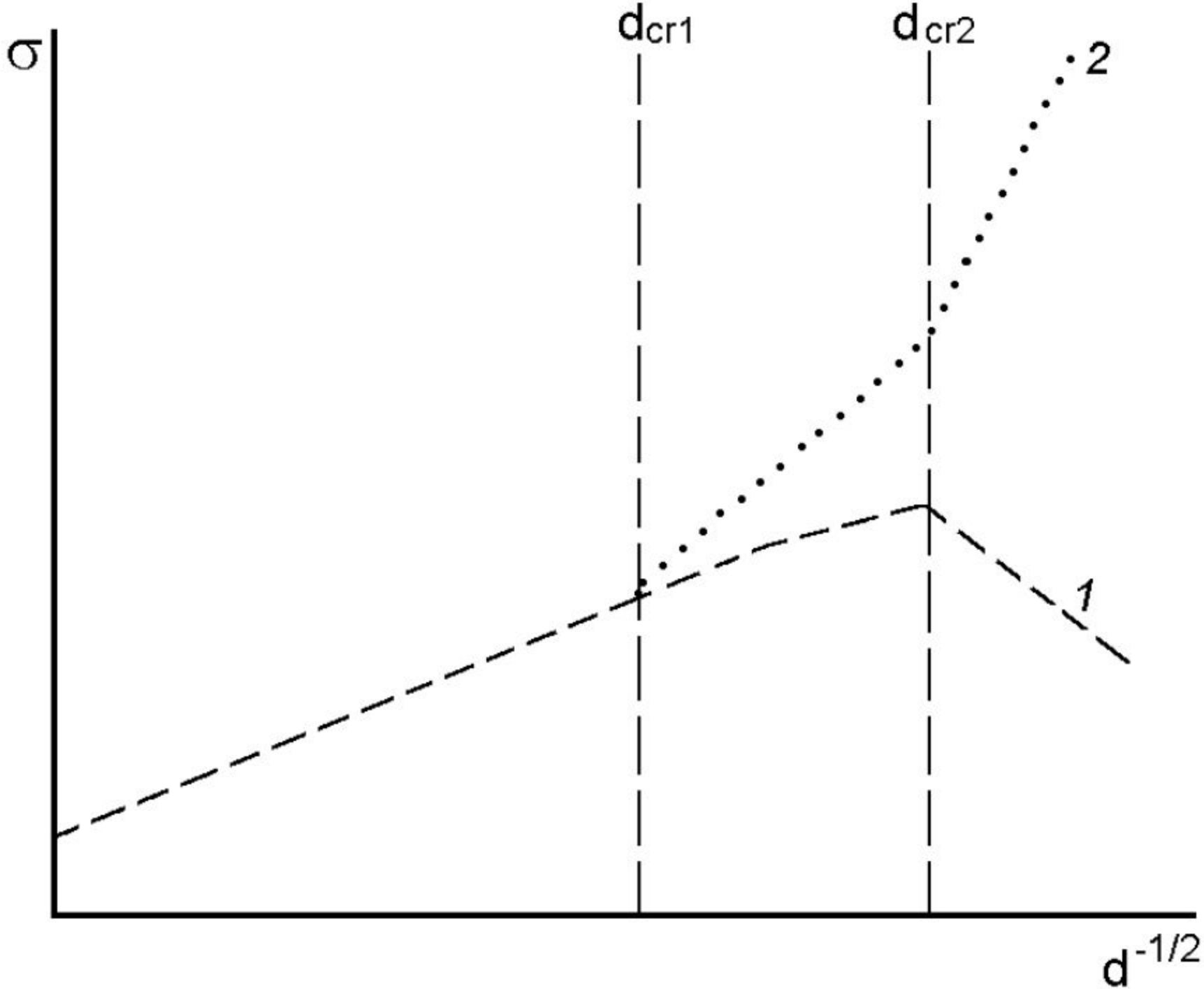
σ
d_{cr1}
d_{cr2}
2
1
$d^{-1/2}$